Osnabrück University
Institute for Cognitive Science

The Role of Feedback in Inter-Areal Communication Mediated by Synchronized Neural Oscillations Studied Using Spiking Model Neurons with Hodgkin-Huxley Ionic Channels

presented to achieve the
Bachelor's degree of Cognitive Science

Jan Zerfowski

Supervised by Prof. Dr. Paul Tiesinga
Second Supervisor Pascal Nieters

August 2019

Abstract Most commonly, cortical neurons with similar functions can be found organized into local groups, that often exhibit intrinsic oscillatory characteristics by the finely adjusted interplay of pyramidal cells and interneurons, often in the gamma frequency-range (30–100 Hz). The effect of a stimulus on the firing rates of a site is highly dependent on the overall oscillatory phase of the circuit upon arrival of the stimulus. This mechanism also constrains the information transfer between cortical sites and it has been hypothesized that attention modulates information transfer in cortex employing this oscillatory mechanism. Here, we model two circuits consisting of cortical pyramidal cells and interneurons that exhibit intrinsic gamma oscillations. We apply external noise stimuli and modulate excitatory feedforward and feedback connections between the circuits. This allows us to investigate the role of feedback connections in synchronization and information transfer between the circuits. We report a positive correlation between feedback connections and regimes of high coherence. Further, feedback connections increase the information transfer in the direction of the feedback, but do not significantly modulate it in the feedforward direction.

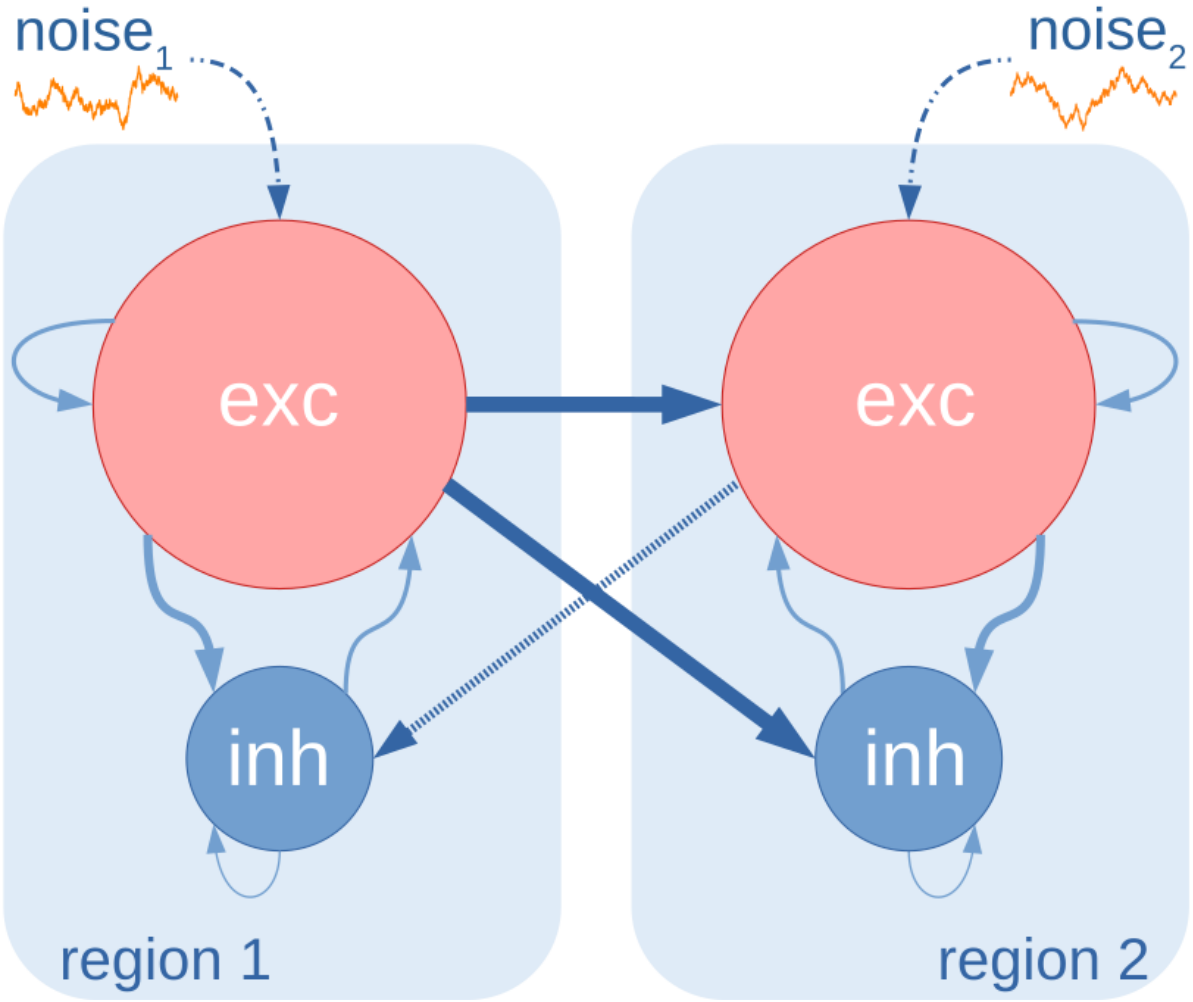

Structure of the network model used in this thesis. The two regions consist of 400 excitatory and 100 inhibitory neurons. Connection strengths and probabilities are indicated by arrow thickness and direction. Feedback is depicted by the dotted arrow. For our investigations of information transfer, independent brownian noise signals are injected into excitatory neurons of region 1 and 2. Figure adapted and used with permission from Frederike Kubandt (personal communication, August 2019).

Contents

1 Introduction

Oscillatory neural activity is an important subject in the Neurosciences, that has been associated with several structural and cognitive functions (see section 1.2). The coordinated rhythmic activity of neurons induce synchronized voltage fluctuations in the brain that can be measured by EEG, MEG and other neuroimaging techniques (Nunez & Srinivasan, 2006). The characterization of these oscillations is based on their location in the brain, frequency, amplitude and power. Mutual interactions between multiple regions then open up a complex network of frequency and phase differences which have been proposed to complement the slow-timescale mechanisms of neural plasticity, like learning and cortical remapping. For processes on faster timescales like attention and motor coordination, rapid opening and closing of communication gateways is necessary, which can be achieved by the synchronization and desynchronization of distinct brain regions. The precise domains in which synchronization between circuits is possible depend on many different factors, such as number and strength of projections between cells, ratio of feedforward and feedback connections, latency, etc. With the Communication Through Coherence (CTC) concept, Pascal Fries built a framework to explain how those emerging macroscopic communication gateways facilitate dynamic coding schemes with effective, precise and selective information transfer for the gamma frequency range (30Hz – 100Hz) (Fries, 2005, 2015).

Due to the vast amount of factors that influence oscillatory behavior, susceptibility of single cells and information transmission between regions, the exact mechanisms still remain elusive and it has proven difficult to construct an overarching framework.

1.1 Prospect of this work

In this thesis, we[1] exploratively investigate the role of feedback connections to fit a missing puzzle piece into the large mix of dependencies that modulate oscillatory behaviour. Based on the research conducted by ter Wal and Tiesinga (2017), we will use a simulated model cortical network with two circuits consisting of pyramidal cells and interneurons with Hodgkin-Huxley ionic channels. We model intra- and interregional AMPA and GABA-synapses in a biologically inspired composition, which allows us to freely modulate the frequencies and strengths of feedforward and feedback connections between the two circuits. We adjust the external driving currents injected into the circuits to keep them in an intermediate gamma frequency range between 35Hz and 67Hz. We first investigate how the oscillation frequency of a circuit is influenced by presynaptic oscillatory activity and feedforward connection strength (section 4.1). We then add feedback connections from pyramidal cells to interneurons to explore how these influence the intrinsic oscillatory activity and the coherence between regions (section 4.2). Further, we argue that the temporal cross-correlation is a sensible measure of information transfer in our delay-coupled system (section 4.3), and then use it to assess the extent to which information transfer can be altered depending on the strength of bidirectional synaptic connections (section 4.4).

Understanding the relationship between feedback connections and information transfer could ultimately lead to novel insights into real biological network structures and better predictions of cortical connectivity from electrophysiological recordings. Understanding the biological and structural origins and effects of neural oscillations may help to find cures for medical conditions such as Parkinson's disease and epilepsy (Buzsáki, Smith, Berger, Fisher, & Gage, 1990). Moreover, the measurement of voluntarily controllable oscillatory activity in motor cortex has already been successfully used to realize a Brain-Computer Interface for a locked-in patient with ALS (Vansteensel et al., 2016) and its medical usefulness is expected to improve in the future (Birbaumer, 2006).

[1] In this thesis, *we* is used to indicate the author's own work. Usage of external results is marked by citations.

1.2 Related work

1.2.1 Historical background

As early as 1875 Richard Caton wrote about finding electrical currents in rabbit and monkey brains (Caton, 1875). Independently, in 1890 Adolf Beck described fluctuating currents in dog and rabbit brains (see Coenen, Fine, and Zayachkivska, 2014 for a review). Vladimir Pravdich-Neminsky (1913) and Hans Berger (1929) found further evidence for cortical oscillations and published the first EEG recordings of animals and humans, respectively.

Since then, many insights into cerebral communication have been gained through EEG, MEG and ECoG measurements. Especially the investigation of epilepsy has uncovered precise details about the inner workings of cortical structures and brain rhythms (Jiruska et al., 2013). The development of antiepileptic drugs has led to many insights into what neurotransmitters and synaptic channels contribute to epileptic seizures and how synchronous behaviour can be altered and dampened (Stafstrom, 2010).

1.2.2 Current hypotheses

It is already known that the exact timing of spikes has effects on synaptic plasticity and long-term potentiation and depression (Feldman, 2012). This spike-timing dependence can lead to the formation and self-organization of neuronal groups which exhibit time-locked and possibly synchronous activity (Izhikevich, Gally, & Edelman, 2004). Already a group of very few neurons can show types of synchronous activity (Elson et al., 1998; Wennekers & Pasemann, 2001), while larger networks can exhibit even more complex behaviors.

The temporally coordinated activity enables the brain to encode information on a higher, macroscopic level which is regulated by different mechanisms. Firstly, the exact timing of incoming spikes plays a role because the oscillations create windows of high input susceptibility (Tiesinga, Fellous, Salinas, José, & Sejnowski, 2004; Gupta, Singh, & Stopfer, 2016; ter Wal & Tiesinga, 2017). Ito and Schuman (2008) have shown that the neurotransmitter dopamine adds a level of regulation by acting as a frequency-dependent neuromodulator, mediating signal-transmission. Many more aspects of information coding are condensed into the popular term *neural coding*, that is subject of current research (Buzsáki & Chrobak, 1995; Singer, 1999; Abbott & Sejnowski, 1999). See also (Cessac, Paugam-Moisy, & Viéville, 2010; Brette, 2018) for a review and discussion of neural coding.

Neural oscillatory patterns occuring in the brain are commonly grouped into frequency bands, namely delta (0.5–4 Hz), theta (4–8 Hz), alpha (8–15 Hz), beta (15–30 Hz) and gamma (30–100 Hz) waves (Wang, 2010; Fries, Nikolić, & Singer, 2007). This classification scheme has been subject to broad discussion and is not challenged here. In this work, we exclusively focus on oscillations in the gamma frequency band. The mechanism of emerging gamma cycles has been described in great detail in (Fries, Nikolić, & Singer, 2007):

> "[A]fter excitatory input, the network of inhibitory interneurons generates rhythmic synchronized activity and imposes rhythmic inhibition onto the entire local network. Pyramidal cells will be able to respond to excitatory input only during the time window of fading inhibition. Because pyramidal cells provide the major excitatory drive to the interneurons, the interneurons will discharge with some phase delay relative to the pyramidal cells and the resulting network inhibition terminates the firing of both the pyramidal cells and the interneurons. The whole network is inhibited and the next gamma cycle starts anew."

This mechanism is a keystone for the Communication Through Coherence (CTC) theory which explains how Gamma oscillations can render communication *effective*, *precise* and *selective* (Fries, 2005, 2015). Looking at the above cycle, we can easily see where these three motifs

come from: The "time window of fading inhibition" modulates the *effectivity* of spikes during each oscillation period and requires the spike to arrive in a *precise* moment. Further, "[a] postsynaptic neuronal group receiving inputs from several different presynaptic groups responds primarily to the presynaptic group to which it is coherent. Thereby, *selective* communication is implemented through selective coherence." (Fries, 2015). See also (Akam & Kullmann, 2014). These statements have been made considering a large body of experimental and theoretical research and have been backed after their publication (Gupta, Singh, & Stopfer, 2016; ter Wal & Tiesinga, 2017).

The described Gamma-cycle above belongs to the Pyramidal-Interneuron Gamma (PING) mechanism which is characterized by the pyramidal cells firing some milliseconds before the interneurons (see also Börgers and Kopell (2005) and Figure 2.4). The literature also describes an Interneuronal Gamma (ING) mechanism, which does not require pyramidal cells (Tiesinga & Sejnowski, 2009). The model network used in this work has also been shown to exhibit the ING motif under certain conditions (ter Wal & Tiesinga, 2017), although we run it exclusively in the PING regime.

Only recently, insight into the effect of feedback connections in such PING networks has been gained. Inhibitory feedback to a model circuit was shown to account for its behavior with in vivo data (Kee, Sanda, Gupta, Stopfer, & Bazhenov, 2015). Doiron, Chacron, Maler, Longtin, and Bastian (2003) showed that in weakly electric fish inhibitory feedback is required to achieve oscillatory behavior only in response to specific stimuli.

1.2.3 Functional roles of neural oscillations

A large body of research exists concerning the purposes and functional roles of neural oscillations. The first association made between behavior and a specific brain rhythm was most likely through the mechanism of alpha blockage that appears when subjects open their eyes, discovered by Hans Berger in 1929 (Karbowski, 2002; Stone & Hughes, 2013). Also so called Central Pattern Generators that produce rhythmic motor patterns (e.g., walking, breathing, flying, swimming) require neural oscillations (Marder & Bucher, 2001). Not only diseases with physical effects such as epilepsy and Parkinson's disease (Buzsáki, Smith, Berger, Fisher, & Gage, 1990) are associated with neural oscillations, but also other disorders such as Schizophrenia (Uhlhaas, Haenschel, Nikolić, & Singer, 2008) and tinnitus (Roberts et al., 2010). These can sometimes be counteracted with high frequency Deep Brain Stimulation (delivering a > 100Hz pulse train to a target brain area) which has also successfully been used to treat chronic and phantom pain, major depression and obsessive-compulsive disorder (Popovych & Tass, 2014). Donner and Siegel (2011) proposed a framework to understand the network differences necessary to realize sensory, motor and cognitive processes in contrast to integrative processes like decision-making.

In this thesis we will only deal with oscillations in the gamma frequency range, which have been associated with visual feature integration (Singer & Gray, 1995), dynamic predictions in top-down processing (Engel, Fries, & Singer, 2001) and working memory (Newman & Grace, 1999; Herrmann, Fründ, & Lenz, 2010). Especially attentional modulation of synchrony (i.e., the increase of coherence between neurons responding to the same stimulus, modulated by attention) has been an important and fruitful research field (Fries, Reynolds, Rorie, & Desimone, 2001; Buia & Tiesinga, 2006; Bosman et al., 2012), which also increased the understanding of oscillatory multiplexing of information (Akam & Kullmann, 2014).

2 Methods

2.1 The model

For our investigations, we simulated two circuits with Hodgkin-Huxley-like model neurons. According to the ratio found in cortex, each circuit consisted of 400 pyramidal cells and 100 interneurons (Markram et al., 2004) (see section 2.2). The neurons were connected using delay-coupled GABA (excitatory, pyramidal cells) and AMPA (inhibitory, interneurons) kinetics with biologically inspired connection probabilites and strengths (see also section 2.2). Interregional connections were only realized from pyramidal cells in the sending circuit to both neuron types in the receiving circuit. Figure 2.1 displays the structure of the whole experimental setup.

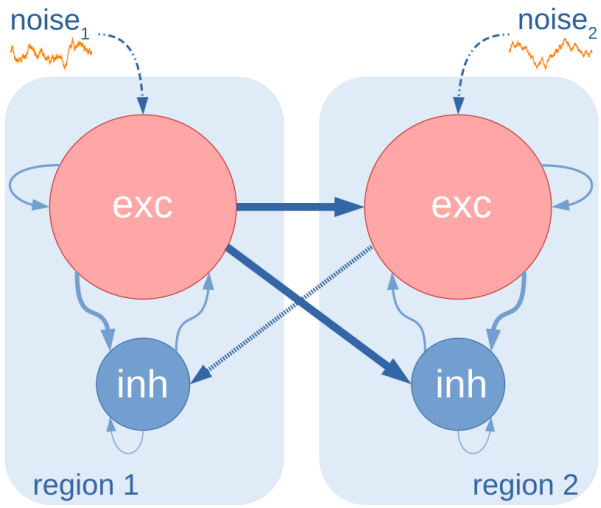

Figure 2.1: Structure of the network model. The two regions consist of 400 excitatory and 100 inhibitory neurons. Connection strengths and probabilities are indicated by arrow thickness (cf. Table 2.1). Feedback is depicted by the dotted arrow. For our investigations of information transfer, independent brownian noise signals are injected into excitatory neurons of region 1 and 2 (section 4.4). Figure adapted from Frederike Kubandt and used with permission (personal communication, August 2019)

The model implementation, simulation and analysis was written for MATLAB, 2019 and was to a large extent adopted from (ter Wal & Tiesinga, 2017). For the integration of the differential equations a 4^{th}-order Runge-Kutta algorithm was used with timesteps $\Delta t = 0.5$ms. To assure both reproducibility and representativity, we used different random number generator seeds (see Appendix A.7). The parallel execution of several simulations was made possible using the Parallel Computing Toolbox (2019b).

2.2 Neuron model

As pyramidal cells, we used the conductance-based single compartment model described by Golomb and Amitai (1997). We call the model's membrane potential V_e (in mV) and it comprises a sodium current I_{Na}, a persistent sodium current I_{NaP}, a delayed rectifier potassium current I_{Kdr} and an A-type potassium current I_{KA}. The sodium and potassium channels are assumed to have fast dynamics. Furthermore, a leak current I_L and GABA and AMPA dynamics are implemented (see Appendix A.1.1 for the channel current dynamics). The injected current is abbreviated as I_{inj} and combines the fixed driving currents as well as noise signal currents (see section 2.3.1). C_m is the membrane capacitance (in µF/cm^2) and $C_m\xi$ is a noise term that is added in each integration step:

$$C_m \frac{dV_e}{dt} = -I_{Na} - I_{NaP} - I_{Kdr} - I_{KA} - I_L - I_{GABA} - I_{AMPA} + I_{Inj} + C_m\xi \tag{2.1}$$

The fast-spiking interneurons were implemented as in (Wang & Buzsáki, 1996) and can be characterized by the following equation:

$$C_m \frac{dV_i}{dt} = -I_{Na} - I_K - I_L - I_{GABA} - I_{AMPA} - I_{inj} + C_m\xi \tag{2.2}$$

Here, again the sodium channel exhibits fast dynamics and its gating variables are replaced by their asymptotic values. The detailed equations used in both neuron models and exact parameter settings can be found in Appendix A.1.

2.2.1 Synaptic model

Pyramidal cells were modeled to express excitatory GABA connections, interneurons express inhibitory AMPA connections (see Appendix A.1.4). In the following, we use the abbreviations e and i for pyramidal cells and interneurons, respectively.

Connection Type	**Connection Probability**	$\mathbf{g_{unitary}}$ (mS/cm^2)
excitatory → *excitatory* within circuit	0.10	1.2
excitatory → *inhibitory* within circuit	0.20	1.0
inhibitory → *excitatory* within circuit	0.40	12.0
inhibitory → *inhibitory* within circuit	0.60	5.0
reg$_1$ *excitatory* → reg$_2$ *excitatory*	0.05	$0 - 15.0$
reg$_1$ *excitatory* → reg$_2$ *inhibitory*	0.10	$0 - 7.5$
reg$_2$ *excitatory* → reg$_1$ *inhibitory*	0.05	$0 - 2.5$

Table 2.1: The probabilities and unitary synaptic connections strengths within circuits and between circuits. Inspired by (ter Wal & Tiesinga, 2017; Holmgren, Harkany, Svennenfors, & Zilberter, 2003; Thomson & Bannister, 2003; Binzegger, Douglas, & Martin, 2004; Markram et al., 2004; Fino & Yuste, 2011)

Synaptic connections within a region expressed a delay of 1ms and were generated randomly between all neuron types, with probabilities of forming a connection and strengths as given in Table 2.1. Interregional connections were only modelled from pyramidal cells to other pyramidal cells and interneurons, but without outgoing connections from interneurons (i.e., they were purely excitatory). They exhibited a 5ms delay and the connection strength was varied (also Table 2.1). The terms feedforward and feedback connection are used here exclusively for interregional connections. In the following graphs, we refer to the total synaptic conductance, which is calculated for each connection type separately, as

$$g_{tot} = g_{unitary} \cdot p \cdot N.$$

Here, g_{tot}, $g_{unitary}$ and p are the total and unitary synaptic conductance and the connection probability for a specific connection type, respectively. N is the number of presynaptic cells. Total synaptic conductance is also referred to as $g_{2\to1}^{e\to i}$ with sending and receiving region in the subscript and the corresponding neuron types in the superscript. The ratio of total feedforward synaptic conductances $g_{1\to2}^{e\to e}/g_{1\to2}^{e\to i}$ was kept constant at 1. For the investigation presented in this thesis, the characteristics of the feedback connections were modified. Exact settings are stated separately in each case.

2.3 Inputs to the circuits

2.3.1 Driving currents

To influence the intrinsic oscillation frequency of a circuit, each neuron in the circuit was injected with a constant depolarizing current $I_{inj} = I_0 + I_\sigma + I_{noise}$, where I_σ was taken from a Gaussian distribution with 0µA/cm^2 mean and standard deviation of 0.1µA/cm^2. The function of the noise signal term I_{noise} is explained in section 2.3.2. The noise term $C_m\xi$ (see equation 2.1 and 2.2) was drawn for each timestep and neuron independently from a uniform distribution between $-\sqrt{6\lambda/\Delta t}$ mV and $\sqrt{6\lambda/\Delta t}$ mV (see Table A.1).

Since the frequency of the system does not increase linearly with a linear change of injected currents, we used a polynomial fit to induce an approximately linear increase of the circuit's oscillation frequency. We increased the injected current to interneurons I_{inj}^{inh} in a stepwise linear fashion of 40 steps, while changing I_{inj}^{exc} as a dependent variable according to the following equations (both given in µA/cm^2, adapted from ter Wal and Tiesinga (2017)):

$$I_{inj}^{inh} = \texttt{linspace}(0.4, 2.0, 40)$$
$$I_{inj}^{exc} = 0.4652 \cdot {I_{inj}^{inh}}^4 - 1.9860 \cdot {I_{inj}^{inh}}^3 + 3.2879 \cdot {I_{inj}^{inh}}^2 - 1.0623 \cdot I_{inj}^{inh} + 0.7546$$

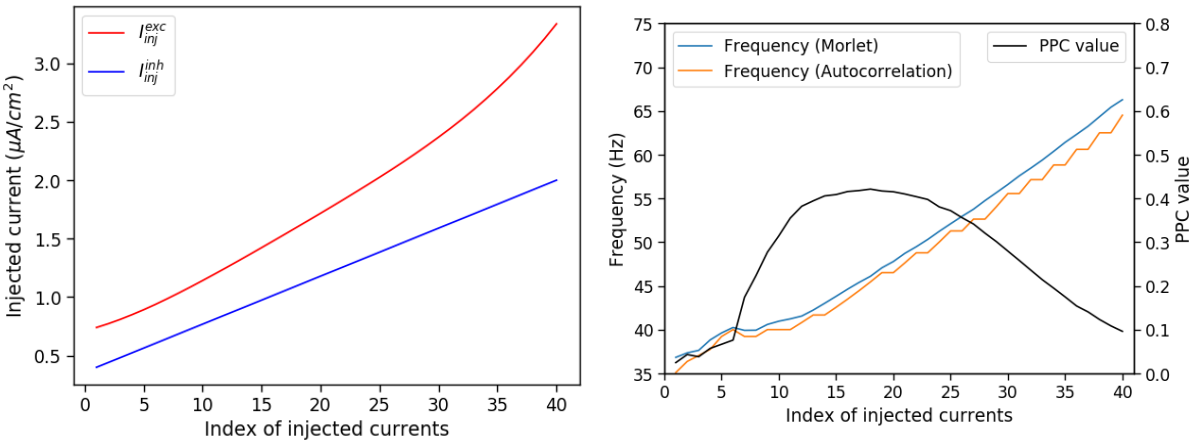

Figure 2.2: Left panel: Injected currents into excitatory (I_{inj}^{exc}, red) and inhibitory neurons (I_{inj}^{inh}, blue). The currents were increased in 40 steps. **Right panel**: The two types of frequency estimation via Morlet wavelets (blue) and autocorrelation (orange) exhibit a systematic difference (discussed in section 2.4.2). The within-circuit-frequency (quantified be the PPC value, section 2.4.3) is depicted in black. The x-values correspond to the injected currents shown in the left panel.

Figure 2.2 demonstrates how the frequency is dependent on the injected currents. For better visibility, we denote only the injected current to interneurons in the other plots of this work, but always also increase the drive to pyramidal cells as described above. It can be seen that for low injected currents the Pairwise Phase Consistency (PPC) (see section 2.4.3) is fairly low. We have empirically observed that for phase locking values below 0.1, within-circuit-synchrony is too low to generate stable oscillations and frequency estimates should be taken with caution. We could not find a perfect fit to induce a linear increase of frequency and therefore take the depicted behavior as our best fit (taken over from ter Wal and Tiesinga (2017)).

2.3.2 Signal noise current

To simulate input to the modeled regions, we generated a brownian noise current implemented as a filtered white noise with an approximate $1/f^2$ amplitude falloff. In chapter 3 - Problems and Solutions we describe how we investigated different noise types to see which one fulfills our requirements in the best way and argue why this slow change is necessary for our work.

The noisy signal currents I_{noise} were injected into the pyramidal cells of both populations for all our investigations of information transfer (see section 4.4). We intended the noise to mediate each

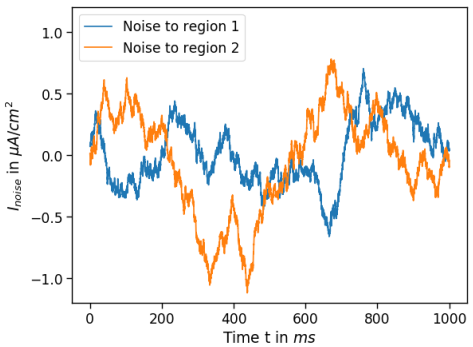

Figure 2.3: Exemplary uncorrelated brownian noise signal currents to region 1 (blue) and region 2 (orange)

cell's firing rate, ultimately leading to changes in the spike density and frequency of the entire population. Each pyramidal cell of a particular region received the same signal trace, while different regions received different signals. The noise signals to region 1 and 2 are hereafter referred to as noise_1 and noise_2, respectively. To make sure that the noise signals to the regions did not carry mutual information that would distort our results, we preselected noise seeds such that the generated noise signals had a correlation $|\rho| \leq 0.05$.

2.4 Data Analysis

2.4.1 Spikes and spike density

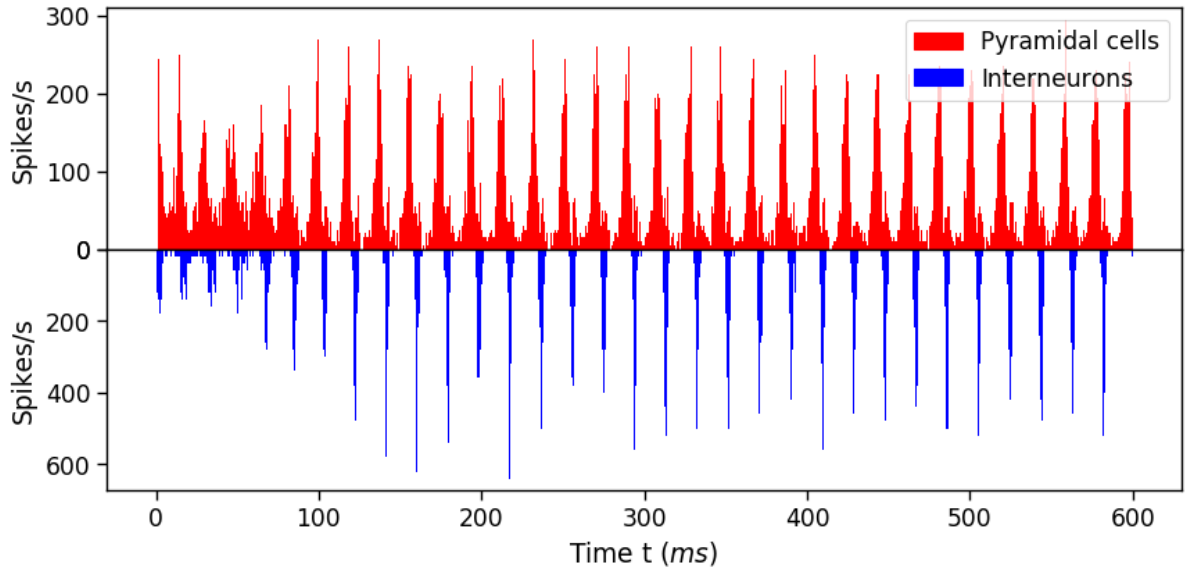

Figure 2.4: Spike density graph with pronounced oscillations, corresponding to the spiketrain in A.1, second panel. The intial period displays a low within-circuit synchrony. After 100ms the oscillations become sharper. The pyramidal cell volleys (red) precede the interneuron volleys (blue) by a few milliseconds (see section 1.2.2).

To determine when a neuron fired a spike, we set fixed membrane potential thresholds. When a pyramidal cell membrane potential exceeded -20mV this was registered as a spike. The threshold for interneurons was set to 0mV. For each timestep, time and neuron index were saved. From that data we computed the spike density trace D_{spike} by binning the data into $\Delta t = 0.5$ms bins, corresponding to a sampling frequency of 2000Hz:

$$D_{spike} = \frac{1000}{N\Delta t} \sum_i X_i(t),$$

$$X_i(t) = \begin{cases} 1 & \text{if } \exists j \; t_j^i \in [t, t+\Delta t] \\ 0 & \text{otherwise} \end{cases} .$$

Here, t_j^i is the time of the j^{th} spike of neuron i. N is the number of neurons in the region, with separate D_{spike} for interneurons and pyramidal cells (see ter Wal and Tiesinga, 2017). Figure 2.4 depicts a spike density graph, a corresponding spiketrain scatterplot can be found in the appendix (Figure A.1, second panel).

To determine the information transfer (see section 2.4.5), the instantaneous firing rate for each region was computed, which was implemented using a sliding average window with the length of one oscillation period on the spike density, taking into account only the current and

anticipatory points of the signal trace (acausal filter). The acausality introduces a systematic bias to our measurements which we discuss in section 3.4. We will subsequently also term the instantaneous firing rate of regions 1 and 2, r_{reg_1} and r_{reg_2}, respectively. The period length was computed using the definition of the oscillation frequency for the corresponding circuit (see section 2.4.2) The signal was smoothed afterwards with a moving average kernel with the length of one oscillation period utilizing the `smooth`-function from the MATLAB Curve Fitting Toolbox (2019a). The whole procedure was adapted from ter Wal and Tiesinga (2017) and can be found in `matlab/analysis_scripts/AnalysisInfo.m` (see also Digital appendix - A.7).

2.4.2 Frequency

In this work, the essential feature to characterize the activity of each region is its frequency. As the regions show interaction effects and injected noise modulates the firing frequency of each neuron, the frequency of a circuit varies over time in each simulation. To quantify this change, we used a measure that can account for such variable frequencies, namely a wavelet transform using the complex Morlet wavelet,

$$\Psi(t) = \frac{1}{\sqrt{\pi f_b}} e^{i2\pi t} e^{\frac{-t^2}{f_b}}.$$

The frequency bandwith f_b was set to 1Hz and we applied it to the pyramidal cell spike density trace, utilizing the function `cwt` from the MATLAB Wavelet Toolbox (2019d). As the scale parameter the previously determined frequency with the autocorrelation technique (see below) was used. `cwt` returns the instantaneous phase trace that is then transformed to an instantaneous frequency trace. These analysis steps were taken over from ter Wal and Tiesinga (2017). The wavelets are centered around $\Delta t = 0$ms and therefore also incorporate anticipatory values in the analysis (non-causal filter). The oscillation frequency of a population is then defined as the mean value of the instantaneous oscillation frequency (see `matlab/analysis_functions/freq_phase.m`). Because unwanted effects might occur due to starting conditions, we discarded the first 200ms from analysis. When the oscillations are not very pronounced, which corresponds to low PPC values (see section 2.4.3), the instantaneous frequency estimate becomes unreliable.

An alternative way to determine the oscillation frequency (but not the instantaneous frequency) is to compute the autocorrelation of the spike density trace and then take the mean distance between its peaks as the period length. The autocorrelation technique yields consistently (about 2Hz) lower values (cf. Figure 2.2, ter Wal and Tiesinga, 2017). We could not find an explanation for this phenomenon, but hypothesize that this might be due to the method used to transform the phase trace to the frequency, which leaves out *abnormal behaviours* (according to the documentation, cf. `matlab/analysis_functions/freq_phase.m`). To remain consistent, we used the frequency trace determined by the wavelet transform in all analyses.

2.4.3 Pairwise Phase Consistency

To measure the strength of intraregional synchronization we used the Pairwise Phase Consistency (PPC) (Vinck, Battaglia, Womelsdorf, & Pennartz, 2012; Vinck, van Wingerden, Womelsdorf, Fries, & Pennartz, 2010). The PPC has been shown to be unbiased and independent of frequency or spike count, such that we can compare the internal synchrony for different conditions. To compute this measure of phase locking, for each possible pair of spikes, the inner product of the two phases in the complex plane is computed and averaged over all pairs. This yields a value between 0 (no synchrony between the spikes in one circuit) and 1 (perfect synchrony, all spikes occur at the same phase). We evaluated the PPC on the pyramidal cell spike density trace, although it has been shown that the analysis for interneurons yields similar, but higher values (ter Wal & Tiesinga, 2017) which is in line with experimental results in cortical circuits (Hasenstaub et al., 2005).

2.4.4 Coherence measure

The magnitude-squared coherence is a measure popularly used to quantify the phase- and frequency-relationship between two signals (i.e., we use the spike density traces of the two regions to quantify synchronization). We used tapers from the Slepian sequences with a time-bandwith product (TW) of 30 to improve the power spectrum estimates (Thomson, 1982). We utilized $2 \cdot \mathrm{TW} - 1$ tapers; the first 4 Slepian sequences are pictured in Figure 2.5. The signal x is multiplied with each of the tapers and the fourier spectrum is computed, yielding $X_k(f)$ as the spectrum for the k^{th} taper.
The multi-taper coherence is defined as

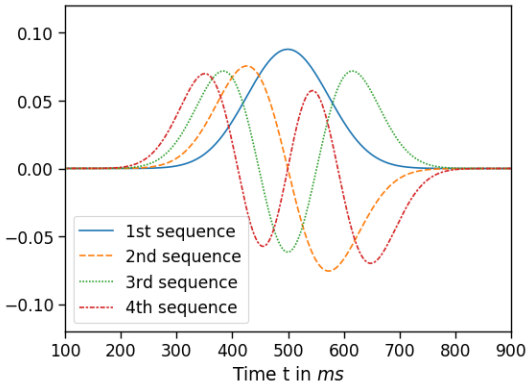

Figure 2.5: First 4 Slepian sequences for 1 second with a Time-Bandwidth product of 30

$$C_{XY}(f) = \frac{|\sum_k X_k(f) \cdot Y_k^*(f)|^2}{\sum_k |X_k(f)|^2 \sum_k |Y_k(f)|^2}$$

and can take values $0 \leq C_{XY}(f) \leq 1$ where 0 means that the signals are completely unrelated and 1 corresponds to full synchrony. Here, X and Y are the spike density histograms of the pyramidal cell population of region 1 and 2, respectively. The sampling rate for the histograms was 2000Hz. To determine a single coherence value, the frequency f of region 1 was taken. To avoid transient effects due to initial conditions, the first 200ms were clipped off for the analysis. The analysis steps were adapted from ter Wal and Tiesinga (2017). Ter Wal and Tiesinga (2017) found that high coherence ($C_{XY} \geq 0.9$) empirically corresponds well to conditions where the frequencies of region 1 and 2 differ by less than 0.05Hz. To compute the multi-taper coherence, the function `coherencyc` from the open source MATLAB toolbox Chronux (Bokil, Andrews, Kulkarni, Mehta, & Mitra, 2010) was used.

2.4.5 Information transfer

A main objective of this work was to quantify the transfer of information between two signals. As signal types we had to analyze both irregular (noise signal) and periodic (spike density of the circuits) data. By using the aforementioned instantaneous firing rate (section 2.4.1) and instantaneous frequency (section 2.4.2), we had two non-periodical measures available for our analyses. We took advantage of the fact that a changing injected current (i.e., a noise signal, see section 2.3.2) into pyramidal cells changes the circuit's instantaneous firing rate and frequency, as has been used by (ter Wal & Tiesinga, 2017) before.

We were interested in how much of the behavior of noise_1 is mirrored by region 2 and, with the introduction of feedback connections, how much of the behavior of noise_2 can be found in region 1. To quantify this share of information between two signals x and y it is common to use the correlation coefficient defined as

$$\rho = \frac{\sum_i (x_i - \bar{x})(y_i - \bar{y})}{\sqrt{\sum_i (x_i - \bar{x})^2} \sqrt{\sum_i (y_i - \bar{y})^2}}. \tag{2.3}$$

Using the correlation coefficient between region 1 and region 2 (as done by ter Wal and Tiesinga (2017)) to quantify information transfer was not possible for us, because we added feedback connections which could **a)** interfere with the way how information is transferred between region 1 and 2 and which **b)** possibly open a reverse pathway for information flowing from region 2 to region 1.

By design of our system, noise_1 and noise_2 are independent from each other (see also section 3.3) and cannot be influenced by the circuit's activity. We therefore measure the relations between noise_1 and region 2 and noise_2 and region 1 to assess information transfer between the regions, as the information injected by noise_1 always flows through region 1 before it can reach region 2.

The measures of firing rate per oscillation (section 2.4.1) and frequency (section 2.4.2) use a sliding window that incorporates values in the future for its estimations (acausal filters). This introduces an anticipatory forward-shift in the signal analysis, which is not relevant when analyzing relations between region 1 and region 2 because the shift is applied for both signals. However, the noise signal does not exhibit this temporal shift, introducing a temporal disparity between the signals.

To control for this effect, we balanced different methods against each other (discussed in section 3.4) and finally decided to also evaluate positive delays up to 30ms in our cross-correlation procedure (see below). Due to the interregional delay of 5ms introduced by the synapses plus the delay until the arriving information takes effect, depending on frequency and phase of the circuit, we expect that the exact effective delay cannot be predicted deterministically. However, we predict that the maximum correlation coincides with the moment of maximum information transfer. Therefore, we chose to temporally shift noise and signal trace against each other to determine for which effective delay the most information is transferred.

The cross-correlation is a measure constructed to quantify the relationship for every possible relative displacement of two signals and matches the requirements stated above. We implemented a version of the cross-correlation by computing the correlation coefficient for every temporal delay within $-35\text{ms} \leq \Delta t \leq 30\text{ms}$. These values are based on empirical results we obtained in section 3.4 and section 4.3. A negative temporal delay means that the noise signal temporally leads the region's signal trace. Since we presuppose that the noise leads the signal, the values $\Delta t \geq 0\text{ms}$ are only included to control for the windows used in other analyses as explained above.

In our implementation, points in time where the region's frequency could not be measured due to too blurry oscillations (see section 2.4.2) or when the signals did not overlap, were left out of the analysis. Further, the first 200ms of the signal trace were clipped off to avoid transient effects due to initial conditions. As the correlation function we used `corr`, from the MATLAB Statistics and Machine Learning toolbox (The Mathworks, Inc., 2019c).

We are aware that there are other measures of information transfer which might be useful as well, but due to the limited time frame of this work we did not manage to implement and evaluate them. They are discussed in chapter 5 - Discussion.

3 Problems and Solutions

In the progress of conducting this research project, we confronted several unexpected situations and even though some of them did not contribute to meaningful results, they were all part of the scientific evaluation process and thus we report about them.

3.1 Evaluation of implementation in the BRIAN simulator

We evaluated the possibility to implement the described system in the free and open source spiking neural network simulator BRIAN (Stimberg, Goodman, Benichoux, & Brette, 2014) written in python (Python Software Foundation, 2019). This would have had the advantage that everybody with a python-running platform could have rerun and reproduced our simulations. We found that the platform does not yet support continuous delay-coupled connections, which were necessary for the specified synaptic type (Marcel Stimberg, personal communication, May 2019). We decided that programming a whole framework to implement delay-coupled synapses into BRIAN or evaluating other available synaptic types for their suitability would exceed the scope of this thesis and decided to use and extend the implementation provided to us by ter Wal and Tiesinga (2017) in MATLAB.

3.2 Evaluation of simulation runtime accelerations

Simulating two regions, each containing 500 neurons with $\sim$120 intraregional connections, for 3.2s with timesteps of 0.05ms already results in very long simulation runtimes. Additionally, the PPC analysis (section 2.4.3) compares each pair of spikes within a circuit, which corresponds to an additional $\mathcal{O}(n^2)$ time complexity. We frequently observed conditions with over 10^5 spikes per region. We evaluated different possibilities to speed up the computations, e.g. running the simulations and analyses on a mainframe computer, using different functions in the analysis and parallelizing the processes.

The framework in its original state computed and analyzed $40 \cdot 16$ simulation conditions sequentially. We found that it is possible to separate simulation and analysis and then execute the simulations in parallel. The analysis scripts access the same data structure for each condition, and thus the parallelization of the analysis would have required a major redesign of the utilized scripts. By parallelizing the execution of the simulation, using the `parfor`-loop from the Parallel Computing Toolbox (2019b), we could improve the runtime, using up to four worker threads simultaneously on each workstation. We further wrote some python and bash-scripts to remotely start and monitor the processes and avoid idle times of the machines. For future investigations we deem that an effort should be made to parallelize the analysis and resolve licensing issues to run the program on distributed resources.

3.3 Noise signal types

For our investigation of information transfer, we at first chose brownian noise as signal type. In many cases, we found a high correlation between the noise injected to region 1 and the signal trace of region 2, but we also observed a very high variance in these results. We revised our choice and found that the framework's brown noise generator very often returns strongly correlated noise, leading to similar inputs to region 1 and 2. We generated 10^5 trials of two 3200ms long noise signals with unique randomization seeds. Less than 16% of them showed correlation within $|\rho| \leq 0.05$. The high variance in correlation between two generated brown noise signals can clearly be observed in the right panel of Figure 3.1. We checked for which

seeds we previously ran our simulations and could confirm that for most of the chosen seeds the correlation between noise_1 and noise_2 was far above 0.05, explaining our results.

To investigate the undistorted information transfer without getting biased results through underlying correlations, we evaluated other choices of noise signals and looked at the correlation relations for white and pink noise. We found both to be within the ± 0.05 correlation range in 100% and 96% of all trials, respectively (left and middle panel in Figure 3.1). We repeated some of the simulations with pink and white noise and observed that the effects of pink noise_1 on region 1 were much weaker than for the white noise (left panel in Figure 3.2), disqualifying it as a potential candidate. The much lower value of correlation for pink noise can be explained as follows: It takes time for the system's spike density and intrinsic frequency to follow sudden changes in injected current. The main difference between the pink and brown noise are their power spectra, and in comparison, pink noise contains much more high frequency components than brown noise. Thus, we hypothesize that pink noise with its $1/f$ power relation contains too many strong sudden changes for the system to follow, and therefore it expresses a lower correlation. To confirm our theory, we conducted three simulations with white noise (which by definition has equal intensity over all frequencies) and obtained even lower values close to 0.

We also evaluated how the choice of a noise amplification value (`sett.noiseamp`) could influence information transfer. Contrary to intuition, a low amplification value (0.5) led to higher correlations between noise_1 and region 2 than a high value (1) (right panel of Figure 3.2). We speculate that this is because a strong noise current also strongly modulates the frequency of region 1. This effect is so strong that previously existent entrainment between region 1 and 2 is lost and effectively less information can be transferred. We finally decided to keep using weak brown noise with preselected seeds that yield a low correlation between -0.05 and 0.05.

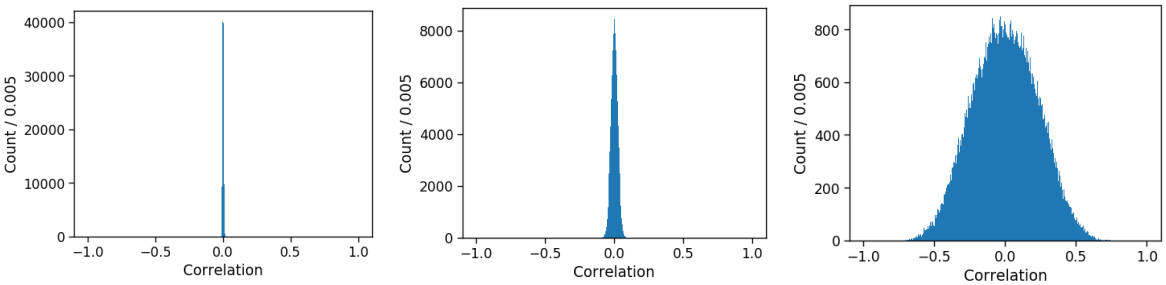

Figure 3.1: Histograms of correlations for 10^5 pairs (3200ms) of each white (left panel), pink (middle panel) and brown noise (right panel).

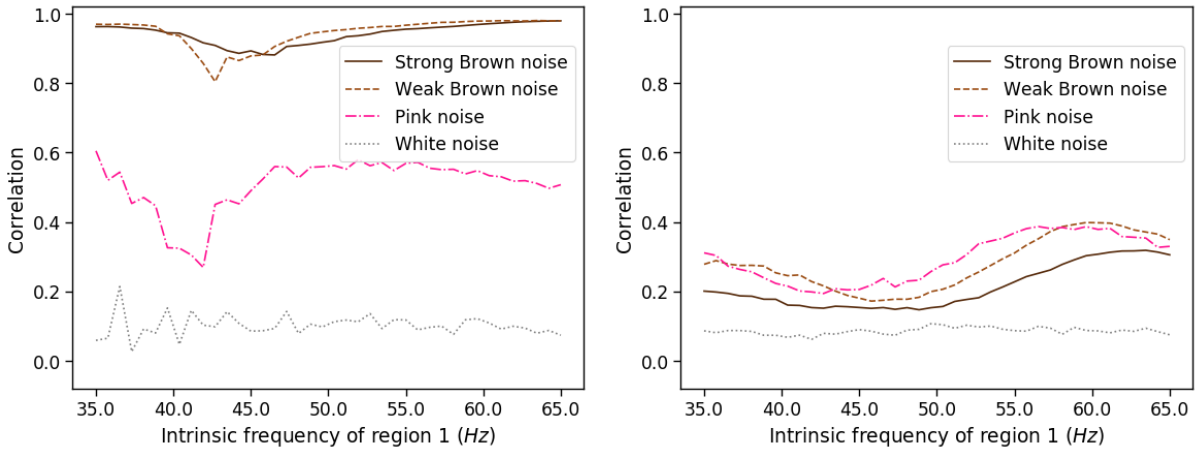

Figure 3.2: Left panel: Mean correlation between noise_1 and firing rate of region 1 for white, pink and brown noise at different intrinsic frequencies of the circuit. **Right panel**: Same as in the left panel, now the correlation is given between noise_1 and region 2.

3.4 Temporal shift due to shifting convolution kernels

The instantaneous firing rate (section 2.4.1) as well as instantaneous frequency (section 2.4.2) are determined by using types of convolution on the original signal. Doing this, the temporal structures of the underlying signal are systematically biased because future values are incorporated into the computation of current values. It has been shown, that this systematic measurement error can distort the results (VanRullen, 2011; Widmann, Schröger, & Maess, 2015). Indeed, we found that the detection of firing rate change sometimes preceded the change in the noise signal (e.g., compare the first 100ms of region 1 in Figure 3.3), which is physically impossible. Since the measures of firing rate and frequency both relate to the ongoing oscillation, they necessitate this type of windowing on the signal and we could not eliminate this requirement.

We evaluated several methods to control for this effect: First, we investigated timeshifting the signals by the window sizes of the used methods. The analysis of the instantaneous firing rate is implemented in such a way, that it considers only future values up to the average period length of the circuit, being determined by $1/f$. Figure 3.3 shows the effect of applying the shift, in this case by $1/54\text{Hz} \approx 18.5\text{ms}$. Here, the signals end up effectively further apart from each other after the shift but, as expected the signal of region 1 then follows the signal of noise_1. For the instantaneous frequency, the `cwt`-function gets the frequency determined by the autocorrelation method $\pm 1\text{Hz}$ as a scale, but centers the Mother wavelet which leads to an anticipation of $1000/2(f-1)\,\text{ms}$.

We found that this technique might correct temporal shifts introduced by the windowing analyses, but it also often leads to a systematic shift away from the delay of highest cross-correlation. As an alternative way we decided to accept the bias, but to extend the window length of the cross-correlation to include positive values. Since the largest possible timeshift could be introduced by the firing rate analysis and the minimum observed frequency was ca. 35Hz, we set the maximum delay analyzed by our cross-correlation technique (section 2.4.5) to a conservative value of $\Delta t \leq +30\text{ms} \approx 1/35\text{Hz}$.

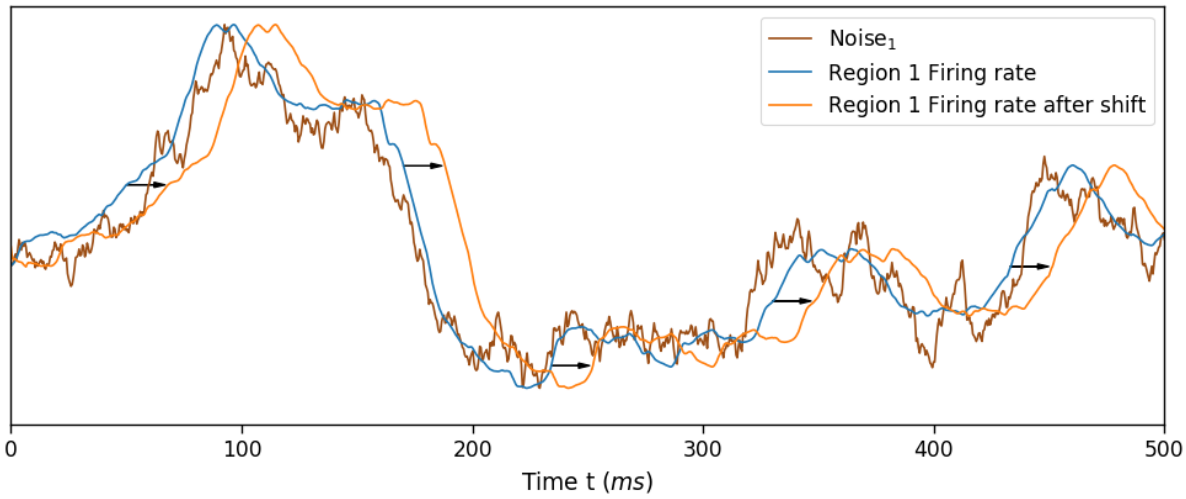

Figure 3.3: Example for a temporal shift of the firing rate signal by the oscillation period length of $1/f$. With the shift (indicated by the black arrows), we attempted to undo the systematic bias introduced by the convolution kernel. In the presented case, the noise signal leads the firing rate after the shift as expected, but we also introduced a bigger gap between the noise and the signal of the region.

4 Results

In the following chapter, we present our findings on the role of feedback connections for coherence and information transfer in the examined model circuits. First, we briefly show the nonlinear effects the feedforward connections from region 1 to region 2 have on the frequency of the latter and that entrainment occurs only in certain conditions (section 4.1). We then add feedback connections from region 2 pyramidal cells to region 1 interneurons and investigate, how these mediate frequency differences and coherence between the two (section 4.2). In section 4.3, we demonstrate that the temporal cross-correlation is a sensible measure to quantify the information transfer between the regions. Finally, we inject uncorrelated brownian noise currents as signals into region 1 and 2 to measure how much of the variance in each region's firing rate and frequency can be explained by the noise injected into the respectively other region when adding different strengths of feedback connections to inhibitory interneurons (section 4.4).

4.1 Manipulation of oscillation frequency through feedforward and feedback connections

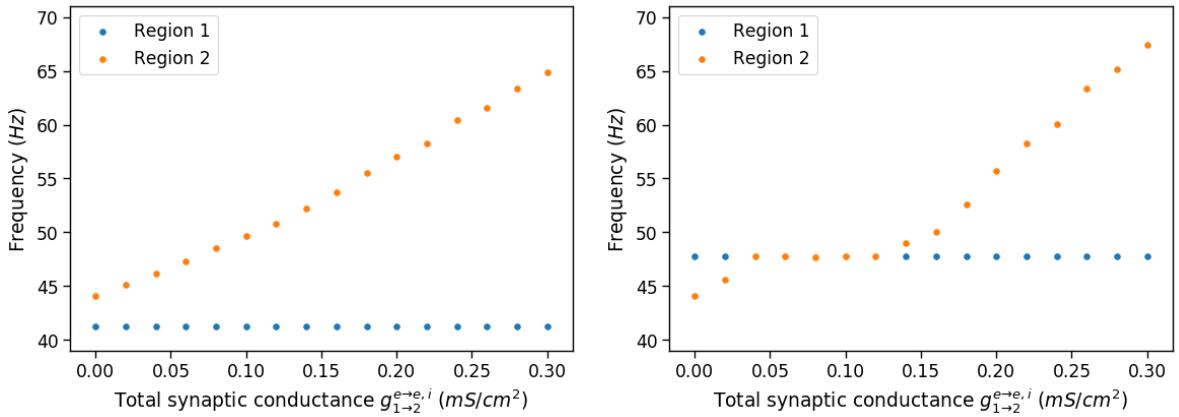

Figure 4.1: Increasing the total synaptic conductance from region 1 to region 2 increases the oscillation frequency of region 2. **Left panel**: Trend of the frequency of region 2 as a function of synaptic conductance, for an initial condition where $f_{reg_1} = 41.5\text{Hz} < f_{reg_2} = 44.2\text{Hz}$. **Right panel**: As in left panel, but $f_{reg_1} = 47.8\text{Hz} > f_{reg_2} = 44.2\text{Hz}$. Entrainment of region 2 by region 1 occurs.

To understand the dynamics of the system, we first looked at how different feedforward connection strengths from region 1 to region 2 affect the system's frequency relations. We tested this by keeping the injected currents to region 1 constant, thereby fixing its frequency at 41.5Hz (left panel of Figure 4.1) or 47.8Hz (right panel). The intrinsic oscillation frequency of region 2 was set to 44.2Hz. We then increased the synaptic conductance linearly for both $e \to e$ and $e \to i$ feedforward connections simultaneously to up to 0.3mS/cm^2. By fixing all other parameters, we could determine the effect on region 2 due to feedforward synapses in the system. Increasing the synaptic conductance corresponds to

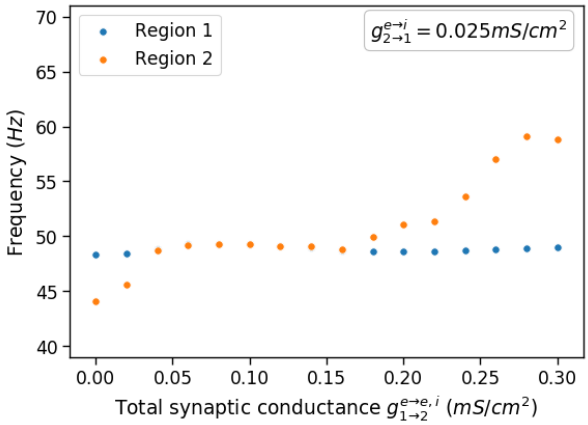

Figure 4.2: Feedback connections from region 2 excitatory to region 1 inhibitory cells added, with $g_{2\to1}^{e\to i} = 0.025\text{mS/cm}^2$. Entrainment occurs for a wider range of feedforward connections than in Figure 4.1 and region 1 frequency is slightly increased.

the increase of mean and amplitude of an oscillating current with the frequency of region 1. We found that, when in the initial condition $f_{reg_1} < f_{reg_2}$, the frequency of region 2 increases almost linearly with the synaptic conductance up to ca. 65Hz (left panel of Figure 4.1). We did not see any synchronization between the two circuits. Instead, the increase of conductance acts similar to the increase of a constant injected current.

In the second condition we started with a slightly higher frequency of region 1, such that $f_{reg_1} > f_{reg_2}$ (right panel of Figure 4.1). Interestingly, in the range from 0.04mS/cm^2 to 0.12mS/cm^2 region 1 entrains region 2 to its frequency. For higher conductances, the frequency of region 2 rises with a steeper slope (compared to the left condition) to up to about 67Hz.

We were then interested in the effect of adding synaptic feedback to this configuration. For this investigation we kept the settings as in the right panel of Figure 4.1, but added feedback connections from region 2 pyramidal cells to region 1 interneurons with 0.025mS/cm^2 (Figure 4.2). The resulting range of entrainment is significantly longer, reaching from 0.04mS/cm^2 to 0.16mS/cm^2 and f_{reg_1} is very slightly increased in that range compared to its baseline frequency. The region 2 frequency rises with higher synaptic conductance, but less fast and not linearly to at most 58Hz. For higher feedback conductances we found the range of entrainment to be even wider with a stronger increase of the frequency of region 1. Demonstrations of this can be found in Figure A.2 in the appendix. This effect of the feedback connections made us interested in how far feedback can increase the synchronization between the two regions and what influence this can have on information transfer. We shall explore these questions in the following sections.

4.2 Modulation of coherence through feedback to inhibitory neurons

Our principal investigation focused on the effects of excitatory feedback connections onto inhibitory neurons. We therefore introduced synaptic connections from pyramidal neurons in region 2 to interneurons in region 1, in addition to the previously established feedforward synapses. In all simulations, region 2 was injected with fixed currents $I^e_{inj} = 1.5\mu A/cm^2$ and $I^i_{inj} = 0.95\mu A/cm^2$ which keeps it in a stable synchronized state with a frequency of about 43.5Hz. The depolarizing curent to region 1 was altered to vary its frequency between 35Hz and 65Hz (see section 2.3.1). The connection probabilities were the same as for the feedforward connections and we varied the total synaptic conductance $g^{e\to i}_{2\to 1}$ between 0mS/cm^2 and 0.1mS/cm^2, corresponding to 1/3 of the maximum total synaptic conductance of the feedforward connections (i.e., 0.3mS/cm^2 for both $g^{e\to e}_{1\to 2}$ and $g^{e\to i}_{1\to 2}$).

When there is no connection at all between the two regions (Figure 4.3, upper left panel at $g^{e\to e,i}_{1\to 2} = 0$mS/cm^2), the circuits display synchronous oscillations only when the frequency of region 1 matches the frequency of region 2 ($f_{reg_2} = 43.5$Hz) at $I^i_{inj} = 0.95\mu A/cm^2$. The alert reader might have noticed here that the actual value of high coherence appears to be slightly farther to the right. The plot shows a mean over three different noise seeds with relatively high variances. We expect that averaging over more trials would cancel this artifact.

With increased synaptic conductance from region 1 to region 2 (along the y-axis) the system exhibits coherence under a wider range of injected currents, with a slight shift to higher currents. This effect can be explained by an interpretation in which the second region acts as a non-linear oscillator, driven by the oscillatory drive coming from the first circuit. The coherence relation basically resembles a tilted Arnold tongue as has been found by ter Wal and Tiesinga (2017). A regular Arnold tongue occurs for example when a non-linear oscillator such as a pendulum is driven by an oscillatory input with variable amplitude. The higher the amplitude of the drive, the stronger the receiving circuit's frequency is pulled towards the drive frequency and a triangular shape of the coherence relation arises (Tiesinga, 2002; Pikovsky, Rosenblum, & Kurths, 2003). In the present case not only the amplitude of the input increases, but also the

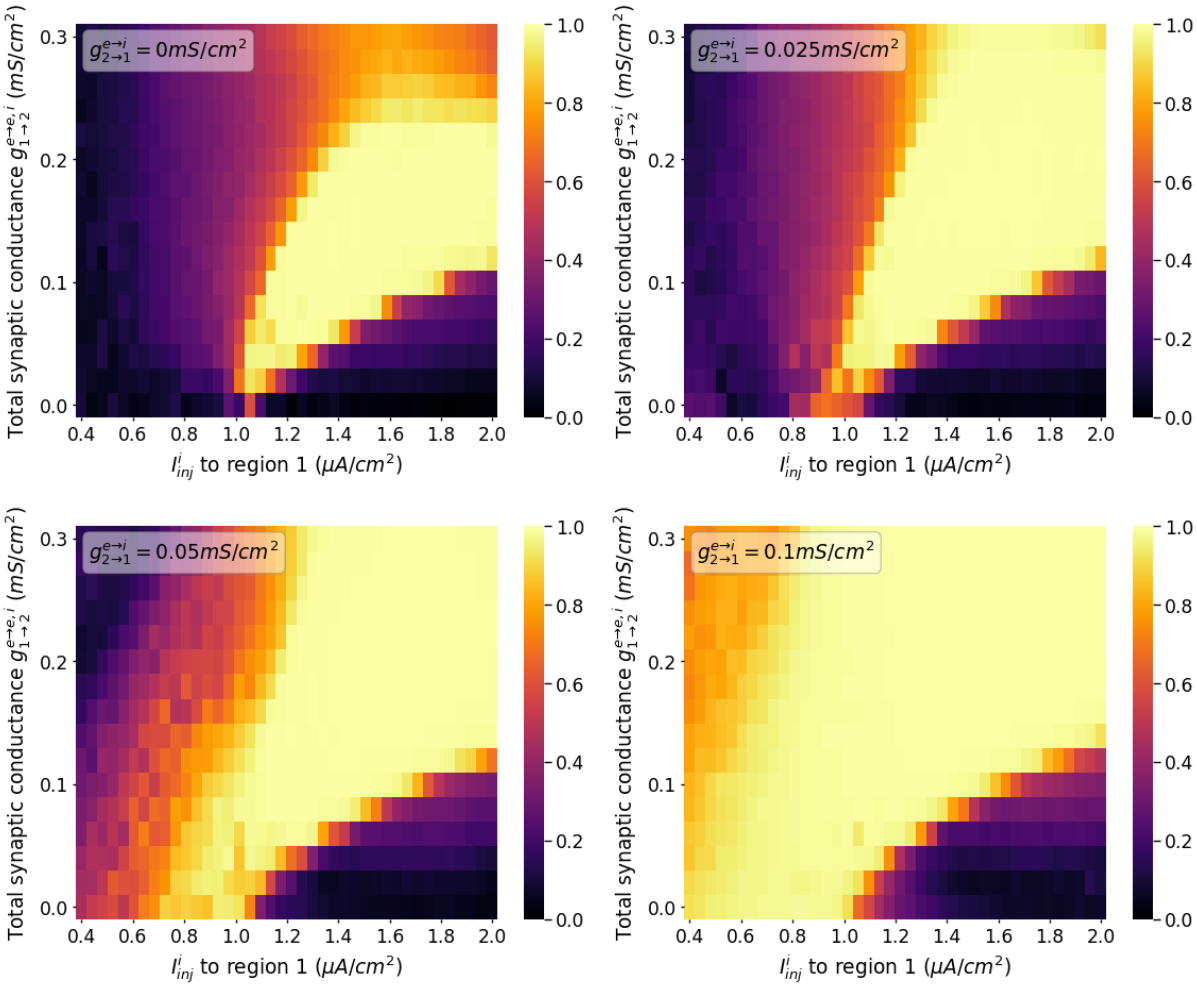

Figure 4.3: Coherence heatmaps for feedforward connection strengths, with fixed inhibitory feedback connections. **Upper left panel**: No feedback connections. A tilted Arnold tongue appears but displays decreasing coherence for $g^{e\to e,i}_{1\to 2} \geq 0.25\text{mS/cm}^2$. **Upper right panel**: $g^{e\to i}_{2\to 1} = 0.025\text{mS/cm}^2$. The Arnold tongue has a triangular shape with clear borders. **Lower left panel**: $g^{e\to i}_{2\to 1} = 0.05\text{mS/cm}^2$. The size of the Arnold tongue increases to a slightly concave triangular shape. **Lower right panel**: $g^{e\to i}_{2\to 1} = 0.1\text{mS/cm}^2$. Strong coherence for an increasingly broad range of injected currents for stronger synaptic feedforward coupling.

average strength. As shown in section 4.1, higher synaptic conductance leads to increased overall input to the second region which in turn raises its frequency. The synchronization range is therefore shifted to the right and a *tilted* Arnold tongue emerges.

For values above 0.25mS/cm^2, the coherence drops again. We found that this drop coincides with the strong decrease of phase locking values for both pyramidal cells and interneurons (cf. Appendix A.5). If the circuits were ordinary non-linear oscillators, the Arnold tongue should continue along its axis. However, as we are dealing with complex dynamics in the system, it is reasonable to expect transient dynamics for extreme settings. The precise origin of this transition remains elusive and should be part of further research.

In the upper right panel of Figure 4.3 we introduced feedback connections from region 2 excitatory cells to region 1 inhibitory cells with a total synaptic conductance of 0.025mS/cm^2. The base of the Arnold tongue appears to widen slightly, the outline straightens and reveals a more triangular shape, being closer to an ideal tilted Arnold tongue than in the 0mS/cm^2 feedback simulation.

The lower left panel of Figure 4.3 represents coherence after the introduction of feedback with a total synaptic conductance of 0.05mS/cm^2. Even for $g^{e\to i}_{1\to 2} = 0\text{mS/cm}^2$, intermediate coherence emerges in a wider range around $I^i_{inj} = 0.97\mu\text{A/cm}^2$ than in the no-feedback condition. We still

observe a tilted Arnold tongue, with its right border slightly farther left, but much wider in comparison to the no feedback condition. The coherence remains persistent for values above 0.025mS/cm^2.

Figure A.2 in the appendix demonstrates that for stronger feedback connections the frequency of region 1 is pulled up towards the frequency of region 2. Further, we can observe that the phase locking values increase and oscillations become more pronounced (Figure A.4). We propose that this is due to the temporally structured excitation of inhibitory neurons, pulling up the frequency of region 1.

In the case of high feedback conductance ($g^{e\to i}_{2\to 1} = 0.1\text{mS/cm}^2$, lower right panel), the regime of high coherence is very large. The inhibition from region 2 pulls up the frequency of region 1 strongly, such that for currents $I^i_{inj} \leq 1.0\mu\text{A/cm}^2$ the system exhibits high coherence when no feedforward connections are present. The regime of synchronization remains in the shape of a tilted Arnold tongue, but is much broader and less sharply decreasing at its left side than in the no feedback condition. For high feedforward conductance ($\geq 0.2\text{mS/cm}^2$) the coherence is strongest and the circuits synchronize for all currents $I^i_{inj} \geq 0.8\mu\text{A/cm}^2$. The formerly tilted tongue now appears like a diagonal club in the heatmap.

In the previously presented results, we observed that an increased feedback connection strength from excitatory to inhibitory neurons facilitates synchronization between the two model circuits. We hypothesize that this facilitation is enabled through the increase of phase locking within the two regions (see Figure A.4) and the frequency increase of region 1:

Naïve intuition would predicts increased activation of region 1 inhibitory cells and therefore an overall decrease of activity and frequency of its pyramidal cells. We propose that the effect we actually observe, an increase of the frequency of region 1, is due to the temporal structure with which region 1 is activated. Region 2 exhibits stable oscillations for almost all conditions with usually higher frequencies than region 1. This implies that region 2 pyramidal cells largely fire within a short period of time in each oscillation. Depending on the feedback connection strength, region 1 interneurons are then more or less strongly driven during a short time window. If the periodic pulses have a suitably similar frequency, they will lead to entrainment of region 1 to the frequency of region 2. This interpretation is in line with other research suggesting that often underlying inhibitory networks facilitate synchronization in such systems (Van Vreeswijk, Abbott, & Bard Ermentrout, 1994; Bartos, Vida, & Jonas, 2007; Cardin et al., 2009).

4.3 Temporal cross-correlation as a measure of information transfer

To investigate how much of the injected information of an input signal is transferred to a receiving circuit, we decided to use the temporal cross-correlation as a measure of information transfer (see section 2.4.5). ter Wal and Tiesinga (2017) chose to use the correlation coefficient, which is equivalent to the cross-correlation at $\Delta t = 0$. However, the correlation coefficient does not suit our needs in this investigation, as it cannot account for the several delays introduced by the system and the analysis: The interregional synapses exhibit a delay of 5ms. Further, we propose that the effective delay could be even larger and depends on the phase of the oscillation, the frequency of the circuit and possibly other indeterministic factors. By design of the analysis, determining instantaneous firing rate and frequency introduces an additional frequency-dependent temporal bias to the signal, which we discussed in section 3.4. We decided to take the cross-correlation as a measure which can take all these uncertainties into account and argue here that it can be used as a measure of information transfer.

It has been shown earlier that the susceptibility of a circuit depends on its phase within the oscillation, so we assume further that for other conditions the effective delay might be larger, up to the time of one full oscillation period. The slowest observed frequency was 35Hz,

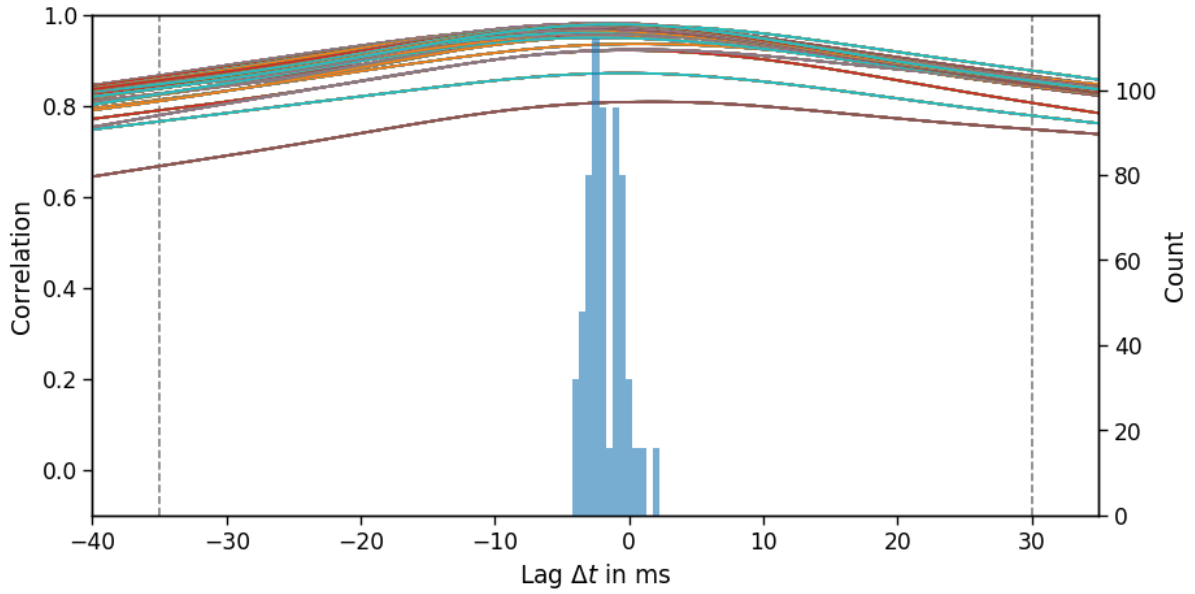

Figure 4.4: Cross-correlation between brownian noise$_1$ and instantaneous firing rate of region 1. The histogram shows the locations of the maxima of the lines. There is a visible peak at $\Delta t \approx -4$ms.

corresponding to a period $T = 1/f \approx 30$ms. Taking also the synaptic delay into account, we chose -35ms as the lower bound for our cross-correlation analyses. As an upper bound, due to the flexible window sizes to up to $\sim$30ms, we analyze the cross-correlation to up to 30ms in advance (see the reasoning in 3.4). We do not attempt to use the cross-correlation as a measure of effective delay here, even though it is theoretically possible after exactly determining and eliminating the bias introduced by the firing rate and frequency analyses. Visually, our procedure shifts the signal against each other until they exhibit the strongest overlap and in this way obtains the maximum correlation coefficient and its corresponding delay.

The lines in Figure 4.4 represent the behavior of the cross-correlation as a function of temporal shift (Δt). Negative values of Δt correspond to the noise leading the signal of region 1. Each line corresponds to one ($g_{1\to2}^{e\to e,i}$, I_{inj})-combination. Lines are only shown for conditions with very high coherence (≥ 0.95) to avoid cluttering. Noise is injected into both regions, no feedback connections are present. The histogram counts the temporal lag of the maximum value for each line.

The cross-correlation between noise$_1$ and firing rate of region 1 peaks at around -4ms. For other analyses, the graphs are very different and cluttered (compare Figure A.3) and can sometimes exhibit the maximum correlation below the -35ms time delay (which then usually correspond to very low correlations). We analyzed the correlation curves for the different tested noise types. Using brownian noise, the curves usually appear relatively flat, due to the slow dynamics of the $1/f^2$ characteristic. Further, we found that the systematic temporal shift introduced in the analysis, in combination with the effective delay almost always cancels the temporal shift between noise current and signal or decreases it to values close to 0ms. However, this is not the case for other noise types and analysis between region 1 and region 2. Figure A.3 demonstrates this for pink noise and analysis of firing rate relations.

4.4 Information transfer with feedback to inhibitory neurons

We have shown previously that feedback to interneurons from region 2 pyramidal cells in some conditions increases the coherence between the regions. Considering the evidence that synchrony can facilitate new communication channels between circuits, we investigated in how far increased synchrony through feedback could mediate the information transfer in our system. As we added

a means of communication directed from region 2 to region 1 just by adding new synaptic connections, we at first explored how much of the information injected into region 2 reaches region 1. We then investigated how the greater regime of coherence acts upon the information transfer from noise_1 to region 2.

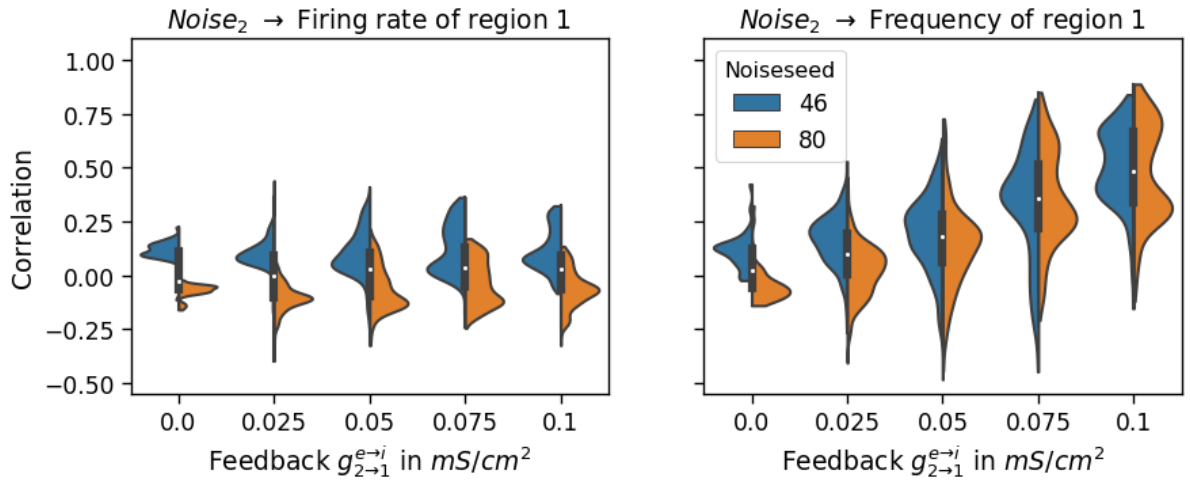

Figure 4.5: Comparison of information transfer measurements from noise_2 to region 1 for two different noise randomization seeds for firing rate (left panel) and frequency (right panel). The correlation between noise_2 and firing rate of region 1 depends on the randomization seed, but stays close to zero even for stronger feedback for both seeds, indicating no information transfer. The correlation in the frequency domain (right panel) increases for stronger feedback to up to a mean value of 0.4.

The left panel of Figure 4.5 shows the information transfer from noise_2 to region 1 with different feedback conductances for two different seeds each. First of all, we confirmed that the channels between region2 and region 1 could possibly convey any information by checking if the information transfer from noise_2 to r_{reg_2} is sufficient. We found $\bar{\rho} \geq 0.8$ for all conditions with very similar distributions, thus a high amount of information is transferred from the noise to the firing rate signal of region 1 (see left panel of Figure A.5). Looking at Figure 4.5 we want to point out the relatively strong difference in the distributions for the two chosen randomization seeds, even though we made sure that the correlation between the noise signals ($\rho_{\text{noise}_1,\text{noise}_2}$) was very low (i.e., $\rho = 0.013$ for seed 46 and $\rho = -0.013$ for seed 80). However, there seems to be a relation between $\rho_{\text{noise}_1,\text{noise}_2}$ and the average of $\rho_{\text{noise}_2,r_{reg_1}}$ (0.12 for seed 46 and -0.07 for seed 80) which cannot be fully ascribed to the very small differences in $\text{noise}_2 \to$ region 2 correlations. To yield more clear estimates and to say for sure where that difference originates, an average over many more unique seeds would be needed. Unfortunately we have to leave this open as a task for further examinations due to time constraints. For stronger feedback, the overall average (marked by the white dots) stays relatively close to zero, while the distributions become broader with largest outliers at around $\rho \approx \pm 0.4$. The averages per seed remain close to their no-feedback counterparts with no systematic increase or decrease, indicating that there is no effect on the instantaneous firing rate owing to increased feedback conductance.

Now looking at the frequency (Figure 4.5, right panel), again the average correlation without feedback is $\rho_{\text{noise}_2,f_{reg_1}} \approx 0$ as expected. Interseed differences appear similar as for the firing rate condition, but with slightly broader distributions. In distinction from r_{reg_1}, there is a positive correlation between feedback strength and information transmission. Even though the distributions become much broader, it is unmissable that the mean correlation $\bar{\rho}_{\text{noise}_2,f_{reg_1}}$ increases. A partial explanation for this effect could be the increasing information transfer from noise_2 to region 2 which is then passed on to region 1. Since this increase happens with a much flatter slope it cannot be the only explanation and we conclude that in fact the

increased synaptic conductance from region 2 pyramidal cells to region 1 interneurons leads to an increased frequency modulation of region 1 through noise$_2$. In summary, we observed an increasing information transfer in the direction of the increasing feedback, exhibited through the instantaneous frequency, but not the firing rate.

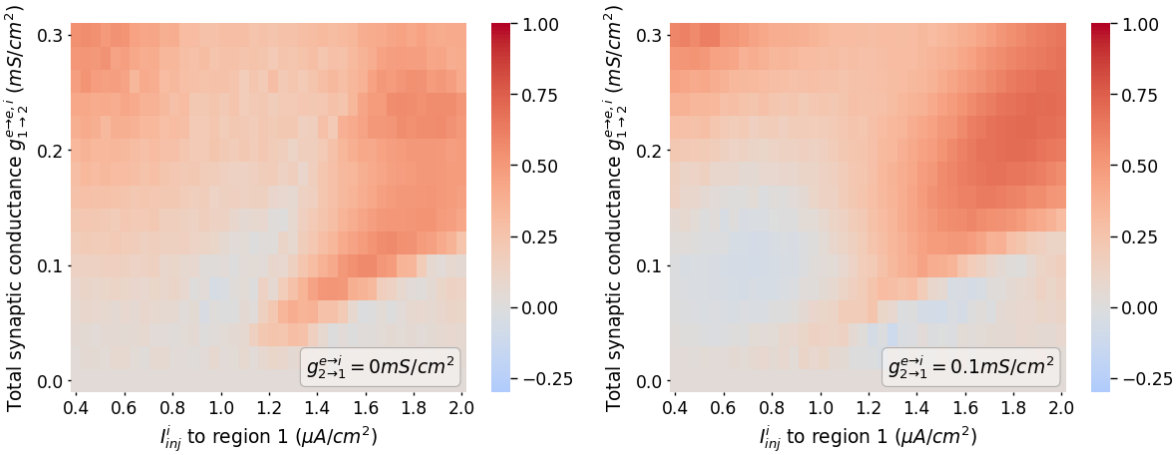

Figure 4.6: Correlation between noise$_1$ and firing rate of region 2 without feedback (left panel) and with strong feedback (1.0mS/cm^2, right panel). Intermediary settings in Figure A.7

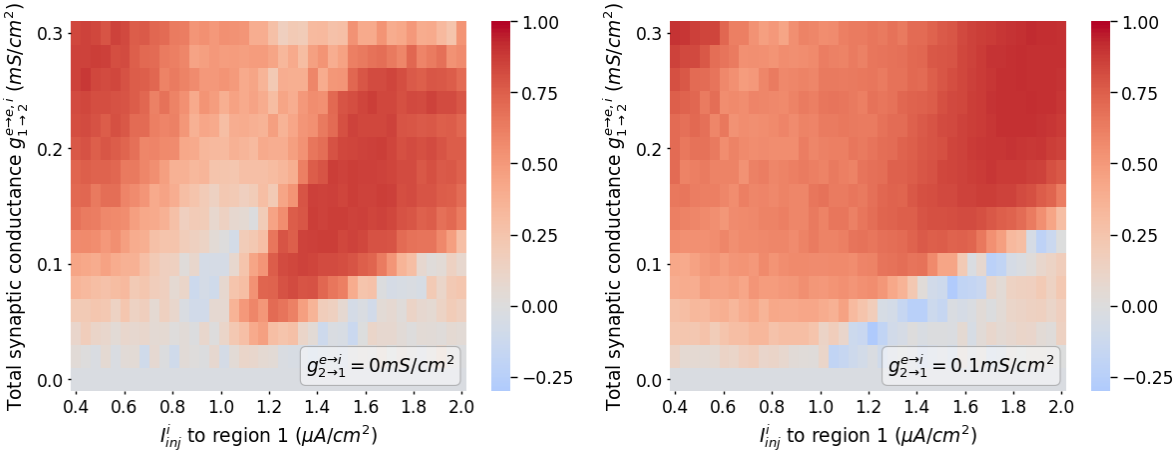

Figure 4.7: Correlation between noise$_1$ and frequency of region 2 without feedback (left panel) and with strong feedback (0.05mS/cm^2, right panel). Intermediary settings in Figure A.7.

In the following paragraphs, we discuss our analyses that could answer another aspect of the question on the role of feedback for information transfer in our network: How could adding connections from region 2 pyramidal cells to region 1 inhibitory neurons modulate the information transfer from region 1 to region 2? We showed earlier that feedback increases the coherence between the two circuits and the theory predicts that higher synchrony enables improved information transfer. To test if there is a positive effect of feedback on feedforward information transfer, we again iterated over different feedback conductances and analyzed how much of the noise signal injected to region 1 reaches region 2 either as modulation of firing rate or instantaneous frequency.

The firing rate correlations are depicted in Figure 4.6. For both conditions, (no feedback (left panel) and strong feedback (right panel, 1.0mS/cm^2)) we can see faint tilted Arnold tongues which overlap with parts of the Arnold tongues we observed for the coherence relations (see Figure 4.3). However, from no feedback to strong feedback the Arnold tongues do not seem to increase in size or strength as they do regarding coherence between the regions. The intermediary

plots shown in the appendix (Figure A.7) do not exhibit much difference, either. Further, the strongest correlation we find is around 0.7 which is not much in comparison to values measured for the frequency (see below). Both plots exhibit a region of slightly higher correlation in the upper left corner, corresponding to low-PPC, low-frequency oscillations of region 1 and intermediate-PPC, high-frequency oscillations of region 2.

We propose that the following mechanism could lead to the emergence of this regime of increased correlation: The low phase locking value of region 1 corresponds to relatively indistinct oscillations with spiking pyramidal cells spread over the whole oscillatory cycle. These oscillations are also much slower than the frequency of region 2, disenabling entrainment and therefore synchronization (cf. section 4.1). The firing rate of region 1 is driven strongly by noise_1 (i.e., high correlation, see Figure A.5). Here, region 1 acts similar to a slowly changing injected current on region 2 excitatory and inhibitory neurons. Since region 2 is already in a stable oscillatory state, the injected current just works during the windows of high susceptibility as a driver for higher firing rates and frequencies. This mechanism works both without feedback and with feedback, as with feedback only the frequency of region 1 is slightly, but not sufficiently, increased and the phase locking value stays small (see Figure A.4) Since the excitatory cells into which the noise is injected connect only weakly to region 2 pyramical cells and more strongly to inhibitory cells, the activity of interneurons might in turn counteract the activation of pyramidal cells and therefore decrease the effect of region 1 activity on region 2 firing rate.

We now turn to our observations regarding frequency changes in region 2 due to noise injected to region 1. Similar to the observations presented for the firing rate, Figure 4.7 reveals high correlations in the form of a tilted Arnold tongue for all feedback conditions. Without feedback, the Arnold tongue area overlaps almost entirely with the regime of high coherence (see section 4.2). To explain that, we consider that region 1 not only entrains region 2, but it also follows the path of the noise with its firing activity and frequency (i.e., high correlation, visible in Figure A.5 and Figure A.6). It is reasonable to say then, that region 2 will follow minor frequency modulations of region 1 and therefore the information transfer is enabled by the upheld synchronization between the two systems. The triangular area (with highest correlation coefficients of ≈ 0.95) is embedded into stripes where almost no information is transferred and sometimes negative correlation values are measured. However, the small absolute values ($|\rho| \leq 0.25$) do not allow to conclude that we have a regime of anticorrelation here, which would be a valid form of information transfer as well.

Again, we observed in the upper left corner an area of high correlation that has a slight oval shape stretching to lower conductance. To explain this, we refer to the proposed mechanism above, in which the low phase locking of spikes from region 1 act like a slowly changing current on region 2 (and not like an oscillatory current): Our circuit is running in the PING regime, therefore interneurons as well as pyramidal cells are important for the emerging frequency. The unsharp oscillations in region 1 drive region 2 without entraining it. The higher the conductance, the stronger the effect on especially interneurons of region 2, due to the connection probability ratio (see Table 2.1). Since the interneurons play an important role in the emergence of oscillatory activity in our system, we propose that their increased activity, paired with the given condition for stable oscillations makes it possible for region 2 to follow the random walk of the noise, communicated by the activity of region 1, with its frequency, leading to high correlation.

For intermediary feedback conditions, the area between the upper left corner and the Arnold tongue decreases in correlation. Only for strong feedback ($\geq 0.075\text{mS/cm}^2$) this reverses but remains to be an area with relatively low correlation, below 0.5. The values in the upper left corner gradually decrease, until there is only high correlation within a small area around $I^i_{inj} = 0.4\mu\text{A/cm}^2$, $g^{e\to e,i}_{1\to 2} = 0.3\text{mS/cm}^2$).

We propose that, even though for stronger feedback frequency and PPC value of region 1 increase, the frequency of region 1 remains too low to entrain region 2 and thus no

5 Discussion

In section 4.1, we presented our observations that synaptic connections between two circuits have the ability to shape their mutual interaction in complex ways. Depending on the frequency difference, entrainment regimes are possible that allow the circuits to synchronize and desynchronize. It was here where we discovered that adding excitatory feedback connections to inhibtiory interneurons can pull up the frequency of the sending region and thereby facilitate synchronization. In section 4.2, we continued exploring this phenomenon and showed that complex interactions between the circuits arise that cannot be explained by ordinary mechanics alone. The emergence of the tilted Arnold tongue is caused by dynamics that exist between two non-linear oscillators, but for example its disappearance for high average and amplitude conditions is not trivial (upper left panel in 4.3). We hypothesized, that this sudden decrease of coherence occurs because of the decreasing intra-circuit synchronization for higher frequencies. However, its true origins remain a challenge for later investigations. We showed that the addition of feedback connections can lead to an increase of phase locking and a counterintuitive increase of the sending circuit's frequency. We ascribed that occurence to the temporal structure of the signal that is fed back to the sending circuit. The increased frequency of the receiving circuit and improved intra-circuit synchronization enable much larger regimes of coherence between the two circuits. Not only is coherence an important concept that can facilitate information transfer, but also the mere synchronization between two cortical circuits carries some kind of information about the two circuits and the nature of their interconnections. It has been hypothesized that inhibitory networks are to large parts responsible for the facilitation of synchronous activity (Hasenstaub et al., 2005). Our results are in line with this, as we showed that feedback to inhibitory cells renders the oscillations more pronounced in both circuits and increases their PPC values.

We propose a system with more than two oscillating circuits that are interconnected in a v-shape such that one region receives signals of two sending circuits. The targeted synchronization and transfer of information is a topic of active research, named oscillatory multiplexing (Akam & Kullmann, 2014). We have seen that, without feedback, the frequency difference is required to be small to facilitate coherence between the circuits. We have shown that the possible frequency difference which still supports synchronization between the regions, increases with feedback. Consequentially, in an imaginary system with multiple regions, feedback connections would allow for much larger frequency differences between the regions, while one circuit could still be flexibly entrained by one of the other circuits, depending on its intrinsic frequency.

From another perspective, exactly that larger regime of possible coherence could be detrimental to the system: When the intrinsic frequencies are all required to lie in a small range, feedback connections could create a kind of competitive entrainment, where each oscillatory frequency alone would be strong enough to entrain the circuit, but as their receiving circuit(s) are driven by multiple oscillations at the same time, it could happen that the whole synchronization scheme breaks down. Thinking further, instead of breaking down it is conceivable that the system becomes sensitive to other signal characteristics, for example the phase difference between the intrinsic oscillation and incoming signals. This could then again render communication selective, precise and effective, which are the main paradigms of the CTC concept by Fries (2015).

Naturally, some limitations apply for the aforementioned results and they should be taken with a grain of salt: First of all, we had limited computational resources available, thus the presented results are each given as an average of two different randomization seeds. For the simulations to determine coherence where no noise currents were injected we did not notice strong seed dependencies, but to obtain reliable results the analyses should be repeated and averaged with different randomization seeds. We also propose that an alternative interneuron or synapse type could be biologically more reasonable to implement feedback connections. We

exclusively modeled the indicated excitatory GABA channels for the feedback communication which validates our results for only this type.

The first part of our work consisted of the analysis and quantification of frequency difference and coherence between the regions mediated by feedforward and feedback connections. In the second part, we established the cross-correlation as a measure of information transfer (section 4.3) to then use it for investigating how synaptic conductance and emerging coherence opens and closes communication channels between the circuits (section 4.4). The inter-regional synapses of our network transmit signals with a delay of 5ms and we assumed that it can take up to one oscillation period until a signal reaches its peak effect (effective delay). The slowest measured frequency in our analyses was around $\approx$ 35Hz and we did conservative approximation of the longest period length with 30ms. The methods we used to analyze the instantaneous frequency and firing rate each utilize a windowing function with the length of one oscillation period, either centered around $\Delta t = 0$ (frequency, non-causal filter) or entirely considering future values $\Delta t \leq {}^{1}/_{f}$ (firing rate, acausal filter), which introduces a systematic temporal shift of the signal, but not the noise. We used the possible effective delay and the anticipatory filtering as theoretical arguments to choose our temporal bounds of the cross-correlation within $-35\text{ms} \leq \Delta t \leq 30\text{ms}$ and take the maximum of this distribution as our information transfer measurement. We observed that for our analyses the maximum value mostly occurs close to $\Delta t = 0\text{ms}$, which we ascribe to the approximate cancellation of the effects from signal analysis and effective delay. When analyzing the cross-correlation between region 1 and region 2, the effective delay is visible more clearly since both signal terms are shifted (see Figure A.3 in the appendix). We deem our approach appropriate to generate estimates of the effective delay between two signals, when previously the bias introduced by the analysis is removed. This could be done by changing the filtering techniques to using causal filters that do not incorporate anticipatory values (Widmann, Schröger, & Maess, 2015).

The cross-correlation is a symmetric measure, not allowing to measure a directedness of information transfer between the regions directly. We therefore computed the noise-to-circuit cross-correlation, which implies a directionality because the noise is independent an thus information can only flow from the noise to the circuit(s). With other measures of information transfer that inherently measure causation (directedness), such as Granger Causality (Granger, 1969) or Transfer Entropy (Schreiber, 2000; Buehlmann & Deco, 2010) it would be possible to quantify the information transferred between region 1 and region 2 and vice versa directly. The simulation results are already available, thus only implementing the algorithms and redoing the analyses would be required to compare different measures of information transfer. We leave this as an open task for future investigation.

Recently, Cole and Voytek published a paper on the *Cycle-by-Cycle Analysis of Neural Oscillations* (2018). Their analysis technique considers the non-linearity and non-stationarity of neural oscillations and also gives information about the waveform symmetry, which might especially be interesting with regard to the application of single, short stimuli.

Finally, we measured the information transfer in different directions for different configurations of feedforward and feedback connections (section 4.4). Depending on the strength of feedback to inhibitory neurons, more information injected through noise_2 is transferred from region 2 to region 1, being expressed in the frequency signal. In the firing rate per oscillation-signal we did not see an increase of information transfer as a function of increased feedback. This seems reasonable, as the feedback connections end in interneurons while we measured the firing rate of the pyramidal cell network. Interneurons are a strong driver of oscillatory behaviour in the PING regime, explaining why increased interneuron activity can accelerate the oscillations and therefore lead to correlation in the frequency domain. Figure 4.5 shows, for two different randomization seeds for the noise generation, that the difference between the results is correlated with the choice of the seed. Thus, a replication of the studies, averaged over far more than two seeds should be done to avoid skewed results due to seed choice.

The result that feedback connections can increase coherence led us to investigate if the information transfer between region 1 and region 2 can likewise be mediated. We computed the maximum cross-correlation between noise_1 and region 2, again for firing rate and frequency. The information transfer to region 2 in terms of firing rate is generally lower than for the frequency, even though the signal of region 1 correlates more strongly in firing rate than in the frequency characteristic with the noise (see A.5 in the appendix). We propose the following mechanism that explains how firing rate change in region 1 could be transformed to frequency change in region 2: A high information transfer between noise_1 and region 1 takes place in the firing rate domain of pyramidal cells into which the noise is injected. A frequency change is caused less strongly (Figure A.6) and with higher dependence on within-circuit synchronization, because interneurons are only subsequently activated. 5ms later, the action potentials caused in the pyramidal cells of region 1 exclusively reach the interneurons of region 2, which in turn fire earlier than usual and thereby increase the oscillation frequency of the circuit (see also Fries, Nikolić, and Singer, 2007).

For both firing rate and frequency, the conditions of high information transfer overlap with the Arnold tongue observed when no feedback is added. Further, we observed an area of high correlation for very low intrinsic frequencies and phase locking values (Figure A.4) (corresponding to unsharp oscillations) and strong feedforward connections (upper left part in Figure 4.6 and Figure 4.7). The low-PPC oscillations in region 1 act more like a constant current following the noise, than like an oscillating current with changing average on region 2. This, in combination with the mechanism proposed above that converts firing rate changes to frequency changes, explains how high correlations between noise_1 and region 2 are possible despite the low correlations between noise_1 and region 1.

We hypothesized earlier, that synchronization between regions could improve information transfer via firing rate and frequency modulations. In section 4.2 we showed that feedback connections enlarge the set of conditions in which coherence between the two circuits emerges. However, the observations we presented in section 4.4 do not support the hypothesized link between coherence and information transfer for the investigated kind of feedback connections. We deem that further studies should be conducted to investigate if the proposed mechanisms of synchronization are working more generally for different structures of oscillating systems or other synaptic types. It could also be interesting to explore if information transfer-enhancing interactions emerge for biologically more realistic feedback configurations.

6 Conclusion

In this thesis, we used two bidirectionally delay-coupled oscillating circuits of model neurons with Hodgkin-Huxley ionic channels to explore the role of feedback in coherence and information transfer. We found that synaptic feedforward connections lead to the emergence of non-linear changes in the receiving circuit, resulting in synchronization (section 4.1) and increased information transfer (section 4.4) between them, which is in line with previous research (ter Wal & Tiesinga, 2017). We evaluated the cross-correlation as a measure of information transfer and used it for our investigations with a time delay between -35ms and 30ms to account for effective delay between the circuits and non-causal filtering methods used in the analysis (sections 3.4 and 4.3). The addition of feedback connections from excitatory pyramidal cells to inhibitory interneurons enables mutual interactions that lead to a strongly enlarged regime of high coherence in the form of a tilted Arnold tongue (section 4.2) and increased within-circuit synchrony (see section 4.2 and Figure A.4). Futher, an increase of information transfer in the direction of the feedback connections is visible in the frequency domain, but not in the firing rate domain. The presented results do not support our hypothesis that feedforward communication is improved by feedback connections through stronger coherence, as we found no change in the frequency or the firing rate domains of information transfer.

This work was conducted using a specific network model with identical GABA dynamics for feedforward and feedback $e \rightarrow i$-connections. For conclusions that are generalizable to the human brain, this choice should be evaluated with respect to its biological plausability. In some cases the presented results display high inter-seed differences; to control for this limitation, repeated simulations with the same settings but different randomization seeds should be run and averaged.

The presented work raises new questions that encourage further research: The cross-correlation can only measure the directed communication because we used the noise signals as input. With inherently directed measures such as Transfer Entropy (Schreiber, 2000; Buehlmann & Deco, 2010) or Granger Causality (Granger, 1969), information transfer could be measured directly from the signals of the two circuits.

It has been shown that oscillations allow multiplexing of information transfer (Akam & Kullmann, 2014; Fries, 2015). To test that motif within our system with feedback conditions, it would be necessary to implement three circuits such that two of them are bidirectionally connected to the third circuit, and modulate their frequencies and phase relations. It is not clear whether the feedback then improves communication by rendering it more exclusive or destroys the entrainment regime, making feedback connections more detrimental than useful.

For further projects utilizing the MATLAB framework we carried over from ter Wal and Tiesinga (2017), an effort should be made to parallelize the analysis scripts and separate the model from the integration algorithm to facilitate the implementation of different neuron or synapse model.

With this research project we contribute a small part to the scientific literature available on oscillations in neural circuits. The effect of excitatory feedback to inhibitory cells with respect to coherence and information transfer has to our knowledge not yet been sufficiently investigated and the exact origins of some properties still remain elusive. Understanding the relationship between feedback connections and information transfer could ultimately lead to novel insights into real biological network structures and better predictions of cortical connectivity from electrophysiological recordings. Gaining knowledge about the complex interactions between oscillating neural circuits represents a crucial step towards finding treatments and therapies for disorders and diseases linked with oscillatory activity in the brain.

7 References

Abbott, L. F. and Terrence Joseph Sejnowski (1999). *Neural Codes and Distributed Representations: Foundations of Neural Computation*. MIT Press. 378 pp.

Akam, Thomas and Dimitri M. Kullmann (Feb. 2014). "Oscillatory Multiplexing of Population Codes for Selective Communication in the Mammalian Brain". In: *Nature Reviews. Neuroscience* 15.2, pp. 111–122. DOI: 10.1038/nrn3668.

Bartos, Marlene, Imre Vida, and Peter Jonas (Jan. 2007). "Synaptic Mechanisms of Synchronized Gamma Oscillations in Inhibitory Interneuron Networks". In: *Nature Reviews Neuroscience* 8.1, pp. 45–56. DOI: 10.1038/nrn2044.

Berger, Hans (Dec. 1929). "Über das Elektrenkephalogramm des Menschen". In: *Archiv für Psychiatrie und Nervenkrankheiten* 87.1, pp. 527–570. DOI: 10.1007/BF01797193.

Binzegger, Tom, Rodney J. Douglas, and Kevan A. C. Martin (Sept. 29, 2004). "A Quantitative Map of the Circuit of Cat Primary Visual Cortex". In: *Journal of Neuroscience* 24.39, pp. 8441–8453. DOI: 10.1523/JNEUROSCI.1400-04.2004.

Birbaumer, Niels (2006). "Breaking the Silence: Brain–Computer Interfaces (BCI) for Communication and Motor Control". In: *Psychophysiology* 43.6, pp. 517–532. DOI: 10.1111/j.1469-8986.2006.00456.x.

Bokil, Hemant et al. (2010). "Chronux: A Platform for Analyzing Neural Signals". In: *Journal of Neuroscience Methods* 192.1, pp. 146–151. DOI: 10.1016/j.jneumeth.2010.06.020.

Börgers, Christoph and Nancy Kopell (Mar. 2005). "Effects of Noisy Drive on Rhythms in Networks of Excitatory and Inhibitory Neurons". In: *Neural Computation* 17.3, pp. 557–608. DOI: 10.1162/0899766053019908.

Bosman, Conrado A. et al. (Sept. 2012). "Attentional Stimulus Selection through Selective Synchronization between Monkey Visual Areas". In: *Neuron* 75.5, pp. 875–888. DOI: 10.1016/j.neuron.2012.06.037.

Brette, Romain (July 13, 2018). "Is Coding a Relevant Metaphor for the Brain?" In: *bioRxiv*, p. 168237. DOI: 10.1101/168237.

Buehlmann, Andres and Gustavo Deco (Sept. 16, 2010). "Optimal Information Transfer in the Cortex through Synchronization". In: *PLOS Computational Biology* 6.9, e1000934. DOI: 10.1371/journal.pcbi.1000934.

Buia, Calin and Paul Tiesinga (June 2006). "Attentional Modulation of Firing Rate and Synchrony in a Model Cortical Network". In: *Journal of Computational Neuroscience* 20.3, pp. 247–264. DOI: 10.1007/s10827-006-6358-0.

Buzsáki, G. and J. J. Chrobak (Aug. 1995). "Temporal Structure in Spatially Organized Neuronal Ensembles: A Role for Interneuronal Networks". In: *Current Opinion in Neurobiology* 5.4, pp. 504–510.

Buzsáki, G. et al. (1990). "Petit Mal Epilepsy and Parkinsonian Tremor: Hypothesis of a Common Pacemaker". In: *Neuroscience* 36.1, pp. 1–14. DOI: 10.1016/0306-4522(90)90345-5.

Cardin, Jessica A. et al. (June 4, 2009). "Driving Fast-Spiking Cells Induces Gamma Rhythm and Controls Sensory Responses". In: *Nature* 459.7247, pp. 663–667. DOI: 10.1038/nature08002.

Caton, Richard (1875). "The Electric Currents of the Brain". In: *British Medical Journal* 2, p. 278. URL: http://digilib.mpiwg-berlin.mpg.de/digitallibrary/jquery/digilib.html?fn=/permanent/vlp/lit27690/pages.

Cessac, Bruno, Hélène Paugam-Moisy, and Thierry Viéville (Jan. 2010). "Overview of Facts and Issues about Neural Coding by Spikes". In: *Journal of Physiology-Paris* 104.1-2, pp. 5–18. DOI: 10.1016/j.jphysparis.2009.11.002.

Coenen, Anton, Edward Fine, and Oksana Zayachkivska (July 2014). "Adolf Beck: A Forgotten Pioneer in Electroencephalography". In: *Journal of the History of the Neurosciences* 23.3, pp. 276–286. DOI: 10.1080/0964704X.2013.867600.

Cole, Scott and Bradley Voytek (Apr. 16, 2018). "Cycle-by-Cycle Analysis of Neural Oscillations". In: *bioRxiv*, p. 302000. DOI: 10.1101/302000.

Doiron, Brent et al. (Jan. 2003). "Inhibitory Feedback Required for Network Oscillatory Responses to Communication but Not Prey Stimuli". In: *Nature* 421.6922, pp. 539–543. DOI: 10.1038/nature01360.

Donner, Tobias H. and Markus Siegel (May 2011). "A Framework for Local Cortical Oscillation Patterns". In: *Trends in Cognitive Sciences* 15.5, pp. 191–199. DOI: 10.1016/j.tics.2011.03.007.

Elson, Robert C. et al. (Dec. 21, 1998). "Synchronous Behavior of Two Coupled Biological Neurons". In: *Physical Review Letters* 81.25, pp. 5692–5695. DOI: 10.1103/PhysRevLett.81.5692.

Engel, A. K., P. Fries, and W. Singer (Oct. 2001). "Dynamic Predictions: Oscillations and Synchrony in Top-down Processing". In: *Nature Reviews. Neuroscience* 2.10, pp. 704–716. DOI: 10.1038/35094565.

Feldman, Daniel E. (Aug. 23, 2012). "The Spike Timing Dependence of Plasticity". In: *Neuron* 75.4, pp. 556–571. DOI: 10.1016/j.neuron.2012.08.001.

Fino, Elodie and Rafael Yuste (Mar. 24, 2011). "Dense Inhibitory Connectivity in Neocortex". In: *Neuron* 69.6, pp. 1188–1203. DOI: 10.1016/j.neuron.2011.02.025.

Fries, P. et al. (Feb. 23, 2001). "Modulation of Oscillatory Neuronal Synchronization by Selective Visual Attention". In: *Science (New York, N.Y.)* 291.5508, pp. 1560–1563. DOI: 10.1126/science.1055465.

Fries, Pascal (Oct. 2005). "A Mechanism for Cognitive Dynamics: Neuronal Communication through Neuronal Coherence". In: *Trends in Cognitive Sciences* 9.10, pp. 474–480. DOI: 10.1016/j.tics.2005.08.011.

— (Oct. 7, 2015). "Rhythms For Cognition: Communication Through Coherence". In: *Neuron* 88.1, pp. 220–235. DOI: 10.1016/j.neuron.2015.09.034.

Fries, Pascal, Danko Nikolić, and Wolf Singer (July 1, 2007). "The Gamma Cycle". In: *Trends in Neurosciences* 30.7, pp. 309–316. DOI: 10.1016/j.tins.2007.05.005.

Golomb, David and Yael Amitai (Sept. 1997). "Propagating Neuronal Discharges in Neocortical Slices: Computational and Experimental Study". In: *Journal of Neurophysiology* 78.3, pp. 1199–1211. DOI: 10.1152/jn.1997.78.3.1199.

Granger, C. W. J. (1969). "Investigating Causal Relations by Econometric Models and Cross-Spectral Methods". In: *Econometrica* 37.3, pp. 424–438. DOI: 10.2307/1912791.

Gupta, Nitin, Swikriti Saran Singh, and Mark Stopfer (Dec. 15, 2016). "Oscillatory Integration Windows in Neurons". In: *Nature Communications* 7. DOI: 10.1038/ncomms13808.

Hasenstaub, Andrea et al. (Aug. 4, 2005). "Inhibitory Postsynaptic Potentials Carry Synchronized Frequency Information in Active Cortical Networks". In: *Neuron* 47.3, pp. 423–435. DOI: 10.1016/j.neuron.2005.06.016.

Herrmann, Christoph S., Ingo Fründ, and Daniel Lenz (June 2010). "Human Gamma-Band Activity: A Review on Cognitive and Behavioral Correlates and Network Models". In: *Neuroscience and Biobehavioral Reviews* 34.7, pp. 981–992. DOI: 10.1016/j.neubiorev.2009.09.001.

Holmgren, Carl et al. (Aug. 15, 2003). "Pyramidal Cell Communication within Local Networks in Layer 2/3 of Rat Neocortex". In: *The Journal of Physiology* 551 Pt 1, pp. 139–153. DOI: 10.1113/jphysiol.2003.044784.

Ito, Hiroshi T. and Erin M. Schuman (2008). "Frequency-Dependent Signal Transmission and Modulation by Neuromodulators". In: *Frontiers in Neuroscience* 2. DOI: 10.3389/neuro.01.027.2008.

Izhikevich, Eugene M., Joseph A. Gally, and Gerald M. Edelman (Aug. 1, 2004). "Spike-Timing Dynamics of Neuronal Groups". In: *Cerebral Cortex* 14.8, pp. 933–944. DOI: 10.1093/cercor/bhh053.

Jiruska, Premysl et al. (Feb. 15, 2013). "Synchronization and Desynchronization in Epilepsy: Controversies and Hypotheses". In: *The Journal of Physiology* 591 Pt. 4, pp. 787–797. DOI: 10.1113/jphysiol.2012.239590.

Karbowski, K. (July 1, 2002). "Hans Berger (1873-1941)". In: *Journal of Neurology* 249.8, pp. 1130–1131. DOI: 10.1007/s00415-002-0872-4.

Kee, Tiffany et al. (Oct. 12, 2015). "Feed-Forward versus Feedback Inhibition in a Basic Olfactory Circuit". In: *PLOS Computational Biology* 11.10, e1004531. DOI: 10.1371/journal.pcbi.1004531.

Marder, Eve and Dirk Bucher (Nov. 27, 2001). "Central Pattern Generators and the Control of Rhythmic Movements". In: *Current Biology* 11.23, R986–R996. DOI: 10.1016/S0960-9822(01)00581-4.

Markram, Henry et al. (Oct. 2004). "Interneurons of the Neocortical Inhibitory System". In: *Nature Reviews Neuroscience* 5.10, p. 793. DOI: 10.1038/nrn1519.

MATLAB (2019). *MATLAB*. Version 9.6.0.1099231 (R2019a) Update 1. Natick, Massachusetts: The Mathworks, Inc.

Newman, James and Anthony A. Grace (June 1, 1999). "Binding across Time: The Selective Gating of Frontal and Hippocampal Systems Modulating Working Memory and Attentional States". In: *Consciousness and Cognition* 8.2, pp. 196–212. DOI: 10.1006/ccog.1999.0392.

Nunez, Paul L. and Ramesh Srinivasan (2006). *Electric Fields of the Brain: The Neurophysics of EEG*. 2nd ed. OCLC: ocm58451867. Oxford ; New York: Oxford University Press. 611 pp.

Pikovsky, Arkady, Michael Rosenblum, and Jürgen Kurths (Apr. 24, 2003). *Synchronization: A Universal Concept in Nonlinear Sciences*. Cambridge University Press. 435 pp.

Popovych, Oleksandr V. and Peter A. Tass (Dec. 16, 2014). "Control of Abnormal Synchronization in Neurological Disorders". In: *Frontiers in Neurology* 5. DOI: 10.3389/fneur.2014.00268.

Pravdich-Neminsky, V.V. (1913). "Ein Versuch Der Registrierung Der Elektrischen Gehirnerscheinungen". In: *Zentralblatt für Physiologie* 27, pp. 951–960.

Python Software Foundation (2019). *The Python Programming Language*. Version 3.7. URL: https://www.python.org/.

Roberts, Larry E. et al. (Nov. 10, 2010). "Ringing Ears: The Neuroscience of Tinnitus". In: *The Journal of Neuroscience* 30.45, pp. 14972–14979. DOI: 10.1523/JNEUROSCI.4028-10.2010.

Schreiber, Thomas (July 10, 2000). "Measuring Information Transfer". In: *Physical Review Letters* 85.2, pp. 461–464. DOI: 10.1103/PhysRevLett.85.461.

Singer, W. (Sept. 1999). "Neuronal Synchrony: A Versatile Code for the Definition of Relations?" In: *Neuron* 24.1, pp. 49–65, 111–125.

Singer, W and C M Gray (Mar. 1, 1995). "Visual Feature Integration and the Temporal Correlation Hypothesis". In: *Annual Review of Neuroscience* 18.1, pp. 555–586. DOI: 10.1146/annurev.ne.18.030195.003011.

Stafstrom, Carl E. (Apr. 2010). "Mechanisms of Action of Antiepileptic Drugs: The Search for Synergy". In: *Current Opinion in Neurology* 23.2, pp. 157–163. DOI: 10.1097/WCO.0b013e32833735b5.

Stimberg, Marcel et al. (2014). "Equation-Oriented Specification of Neural Models for Simulations". In: *Frontiers in Neuroinformatics* 8. DOI: 10.3389/fninf.2014.00006.

Stone, James and John Hughes (Feb. 2013). "Early History of Electroencephalography and Establishment of the American Clinical Neurophysiology Society". In: *Journal of Clinical Neurophysiology* 30.1, pp. 28–44. DOI: 10.1097/WNP.0b013e31827edb2d.

Ter Wal, Marije and Paul H. Tiesinga (Feb. 9, 2017). "Phase Difference between Model Cortical Areas Determines Level of Information Transfer". In: *Frontiers in Computational Neuroscience* 11. DOI: 10.3389/fncom.2017.00006.

The Mathworks, Inc. (Mar. 2019a). *Curve Fitting Toolbox*. Version 7.0. The Mathworks, Inc. URL: https://de.mathworks.com/help/parallel-computing/index.html (visited on 07/18/2019).

The Mathworks, Inc. (Mar. 2019b). *Parallel Computing Toolbox*. Version 7.0. The Mathworks, Inc. URL: https://de.mathworks.com/help/parallel-computing/index.html (visited on 07/18/2019).

— (Mar. 2019c). *Statistics and Machine Learning Toolbox*. Version 11.5. The Mathworks, Inc. URL: https://de.mathworks.com/help/parallel-computing/index.html (visited on 07/18/2019).

— (Mar. 2019d). *Wavelet Toolbox*. Version 5.2. The Mathworks, Inc. URL: https://de.mathworks.com/help/wavelet/index.html (visited on 07/18/2019).

Thomson, Alex M. and A. Peter Bannister (Jan. 1, 2003). "Interlaminar Connections in the Neocortex". In: *Cerebral Cortex* 13.1, pp. 5–14. DOI: 10.1093/cercor/13.1.5.

Thomson, D. J. (Sept. 1982). "Spectrum Estimation and Harmonic Analysis". In: *Proceedings of the IEEE* 70.9, pp. 1055–1096. DOI: 10.1109/PROC.1982.12433.

Tiesinga, P. H. E. (Apr. 2, 2002). "Precision and Reliability of Periodically and Quasiperiodically Driven Integrate-and-Fire Neurons". In: *Physical Review E* 65.4, p. 041913. DOI: 10.1103/PhysRevE.65.041913.

Tiesinga, Paul H. et al. (2004). "Inhibitory Synchrony as a Mechanism for Attentional Gain Modulation". In: *Journal of Physiology, Paris* 98.4-6, pp. 296–314. DOI: 10.1016/j.jphysparis.2005.09.002.

Tiesinga, Paul and Terrence J. Sejnowski (Sept. 24, 2009). "Cortical Enlightenment: Are Attentional Gamma Oscillations Driven by ING or PING?" In: *Neuron* 63.6, pp. 727–732. DOI: 10.1016/j.neuron.2009.09.009.

Uhlhaas, Peter J. et al. (Sept. 2008). "The Role of Oscillations and Synchrony in Cortical Networks and Their Putative Relevance for the Pathophysiology of Schizophrenia". In: *Schizophrenia Bulletin* 34.5, pp. 927–943. DOI: 10.1093/schbul/sbn062.

Van Vreeswijk, Carl, L. F. Abbott, and G. Bard Ermentrout (Dec. 1, 1994). "When Inhibition Not Excitation Synchronizes Neural Firing". In: *Journal of Computational Neuroscience* 1.4, pp. 313–321. DOI: 10.1007/BF00961879.

VanRullen, Rufin (Dec. 7, 2011). "Four Common Conceptual Fallacies in Mapping the Time Course of Recognition". In: *Frontiers in Psychology* 2. DOI: 10.3389/fpsyg.2011.00365.

Vansteensel, Mariska J. et al. (Nov. 24, 2016). "Fully Implanted Brain–Computer Interface in a Locked-In Patient with ALS". In: *The New England journal of medicine* 375.21, pp. 2060–2066. DOI: 10.1056/NEJMoa1608085.

Vinck, Martin et al. (May 15, 2010). "The Pairwise Phase Consistency: A Bias-Free Measure of Rhythmic Neuronal Synchronization". In: *NeuroImage* 51.1, pp. 112–122. DOI: 10.1016/j.neuroimage.2010.01.073.

Vinck, Martin et al. (Aug. 1, 2012). "Improved Measures of Phase-Coupling between Spikes and the Local Field Potential". In: *Journal of Computational Neuroscience* 33.1, pp. 53–75. DOI: 10.1007/s10827-011-0374-4.

Wang, Xiao-Jing (July 2010). "Neurophysiological and Computational Principles of Cortical Rhythms in Cognition". In: *Physiological reviews* 90.3, pp. 1195–1268. DOI: 10.1152/physrev.00035.2008.

Wang, Xiao-Jing and György Buzsáki (Oct. 15, 1996). "Gamma Oscillation by Synaptic Inhibition in a Hippocampal Interneuronal Network Model". In: *The Journal of Neuroscience* 16.20, pp. 6402–6413. DOI: 10.1523/JNEUROSCI.16-20-06402.1996.

Wennekers, Thomas and Frank Pasemann (June 1, 2001). "Generalized Types of Synchronization in Networks of Spiking Neurons". In: *Neurocomputing*. Computational Neuroscience: Trends in Research 2001 38-40, pp. 1037–1042. DOI: 10.1016/S0925-2312(01)00389-7.

Widmann, Andreas, Erich Schröger, and Burkhard Maess (July 2015). "Digital Filter Design for Electrophysiological Data – a Practical Approach". In: *Journal of Neuroscience Methods* 250, pp. 34–46. DOI: 10.1016/j.jneumeth.2014.08.002.

8 Acknowledgements

I would like to express my great appreciation to my research supervisors Paul Tiesinga and Pascal Nieters for their guidance during this project and their useful feedback on my methods and the script. Further, I want to thank Marije ter Wal for providing me with the simulation framework which enabled me to realize this project.
My deep gratitude and thankfulness is expressed towards Frederike Kubandt for her personal support, her invaluable suggestions and the visualization of the network structure.
I am grateful for Niklas Kitzmann's extraordinarily helpful comments and advice which have strongly improved the quality and comprehensibility of this thesis. I want to furthermore thank Anna Lisa Gert, Benedikt Ehinger, Gordon Pipa and Peter König for fruitful discussions and their availability to discuss my methods and problems that occured during writing.
In the Neurosciences, MATLAB is a very important software and, having had no experience whatsoever, I learned a lot during the self-training process. I am especially thankful to everybody who answered my numerous questions on the paradigms and concepts realized in this programming language.

A Appendix

A.1 Neuron and synapse models

The neuron and synaptic equations, as well as their implementations for MATLAB, were taken over from ter Wal and Tiesinga (2017).

A.1.1 Pyramidal cell equations

The membrane potential V_e (in mV) of the 400 excitatory, pyramidal cells (Golomb & Amitai, 1997) in each region obeys:

$$C_m \frac{dV_e}{dt} = -I_{Na} - I_{NaP} - I_{Kdr} - I_{KA} - I_L - I_{GABA} - I_{AMPA} + I_{Inj} + C_m\xi \tag{A.1}$$

The channel currents are defined as follows (the channel types are described in section 2.2):

$$\begin{aligned} I_L &= g_L(V_e - E_L) \\ I_{Na} &= g_{Na} m_\infty^3(V_e) h (V_e - E_{Na}) \\ I_{NaP} &= g_{NaP} p_\infty(V_e)(V_e - E_{Na}) \\ I_{Kdr} &= g_{Kdr} n^4 (V_e - E_K) \\ I_{KA} &= g_{KA} \alpha_\infty^3 b (V_e - E_K) \\ I_{GABA} &= g_{ie} s_{ie}^{tot}(t)(V_e - E_{GABA}) \\ I_{AMPA} &= g_{ee} s_{ee}^{tot}(t)(V_e - E_{AMPA}) \end{aligned} \tag{A.2}$$

Here, a, b, h, m, n, p and s are gating variables. The A-type potassium channel gating variable a, sodium channel gating variable m and persistent sodium channel gating variable p are assumed to have fast dynamics. They were replaces by their asymptotic values a_∞, m_∞ and p_∞. The dynamics of the other gating variables are defined as follows:

$$\begin{aligned} \frac{dh}{dt} &= \frac{h_\infty(V_e) - h}{\tau_h} \\ \frac{dn}{dt} &= \frac{n_\infty(V_e) - n}{\tau_n} \\ \frac{db}{dt} &= \frac{b_\infty(V_e) - b}{\tau_b} \end{aligned} \tag{A.3}$$

The rate constants for the channels are defined as:

$$\begin{aligned} m_\infty &= [e^{-\frac{V_e+30}{0.5}} + 1]^{-1} \\ h_\infty &= [e^{\frac{V_e+53}{7}} + 1]^{-1} \\ \tau_h &= 0.37 + 2.78[e^{\frac{V_e+40.5}{6}} + 1]^{-1} \\ p_\infty &= [e^{-\frac{V_e+40}{5}} + 1]^{-1} \\ n_\infty &= [e^{-\frac{V_e+30}{10}} + 1]^{-1} \\ \tau_n &= 0.37 + 1.85[e^{\frac{V_e+27}{15}} + 1]^{-1} \\ \alpha_\infty &= [e^{-\frac{V_e+50}{20}} + 1] \\ b_\infty &= [e^{\frac{V_e+80}{6}} + 1]^{-1} \\ t_b &= 15\text{ms} \end{aligned} \tag{A.4}$$

The model parameter values appearing in the equations are listed in Table A.1.

A.1.2 Interneuron equations

The membrane potential V_i (in mV) of the 100 inhibitory, fast-spiking interneurons (Wang & Buzsáki, 1996) in each region obeys:

$$C_m \frac{dV_i}{dt} = -I_{Na} - I_K - I_L - I_{GABA} - I_{AMPA} - I_{inj} + C_m \xi \tag{A.5}$$

The channel currents are defined as follows (the channel types are described in section 2.2):

$$\begin{aligned} I_L &= g_L(V_i - E_L) \\ I_{Na} &= g_{Na} m_\infty^3(V_i) h (V_i - E_{Na}) \\ I_K &= g_K n^4 (V_i - E_K) \\ I_{GABA} &= g_{ii} s_{ii}^{tot}(t)(V_i - E_{GABA}) \\ I_{AMPA} &= g_{ei} s_{ei}^{tot}(t)(V_i - E_{AMPA}) \end{aligned} \tag{A.6}$$

Here, h, m, n and s are gating variables. The sodium channel gating variable m is assumed to have fast dynamics and is replaced by its asymptotic value m_∞. The dynamics of h and n are described as follows:

$$\begin{aligned} m_\infty &= \frac{\alpha_m}{\alpha_m + \beta_m} \\ \frac{dh}{dt} &= \phi(\alpha_h(1-h) - \beta_h h) \\ \frac{dn}{dt} &= \phi(\alpha_n(1-n) - \beta_n n) \end{aligned} \tag{A.7}$$

The rate constants for the channels are defined as:

$$\begin{aligned} \alpha_m &= \frac{-0.1(V+35)}{e^{-0.1(V+35)} - 1} \\ \beta_m &= 4e^{-\frac{V+60}{18}} \\ \alpha_h &= 0.07e^{-\frac{V+58}{20}} \\ \beta_h &= [e^{-0.1(V+28)} + 1]^{-1} \\ \alpha_n &= \frac{-0.01(V+34)}{e^{-0.1(V+34)} - 1} \\ \beta_n &= 0.125e^{-\frac{V+44}{80}} \end{aligned} \tag{A.8}$$

The model parameter values appearing in the equations are listed in Table A.1.

A.1.3 Parameters

The parameters of the model were chosen in accordance with (ter Wal & Tiesinga, 2017)

Parameter (Unit)	**Pyramidal Cells**	**Interneurons**
E_L (mV)	-70	-65
E_{Na} (mV)	55	55
E_K (mV)	-90	-90
E_{GABA} (mV)	0	0
E_{AMPA} (mV)	-75	-75
g_L (mS/cm^2)	0.02	0.1
g_{Na} (mS/cm^2)	24	35
g_{NaP} (mS/cm^2)	0.07	-
g_{Kdr} (mS/cm^2)	3	-
g_{KA} (mS/cm^2)	1.4	-
g_K (mS/cm^2)	-	9
C_m (µF/cm^2)	1	1
ϕ	-	5
λ (mV^2/ms)	1	1
Delay within area (ms)	5	5
Delay between areas (ms)	5	5

Table A.1: Parameters used for the differential equations of pyramidal cells and interneurons

A.1.4 GABA and AMPA synapse equations

The equations A.2 and A.6 define the behavior for the connection-type specific synaptic input currents I_{GABA} and I_{AMPA}. The descriptions, equations and implementations are taken over from ter Wal and Tiesinga (2017, supplementary material). They have the general form:

$$I_{syn} = g_{kl} s_{kl}^{tot} (V - E_{syn}) \tag{A.9}$$

with g_{kl} being the unitary synaptic conductance (in mS/cm^2) for connections from presynaptic neuron type k to postsynaptic neuron type l. s_{kl}^{tot} represents the total input to the postsynaptic cell and depends on the network structure and the synaptic gating variables s of the presynaptic cells:

$$\begin{aligned} \frac{ds}{dt} &= \alpha F(V_{pre})(1-s) - \beta s \\ F(V_{pre}) &= [1 + e^{\frac{V_{pre} - \theta_s}{\sigma_s}}]^{-}1 \end{aligned} \tag{A.10}$$

Parameters used in the equations are listed in Table A.2.

Parameter (Unit)	**AMPA**	**GABA**
θ_s (mV)	-20	0
α (ms^{-1})	0.8	10
β (ms^{-1})	0.5	0.2
σ_s (mV)	2	2

Table A.2: Parameters used for the AMPA and GABA dynamics

A.2 Histograms for high and low PPC values

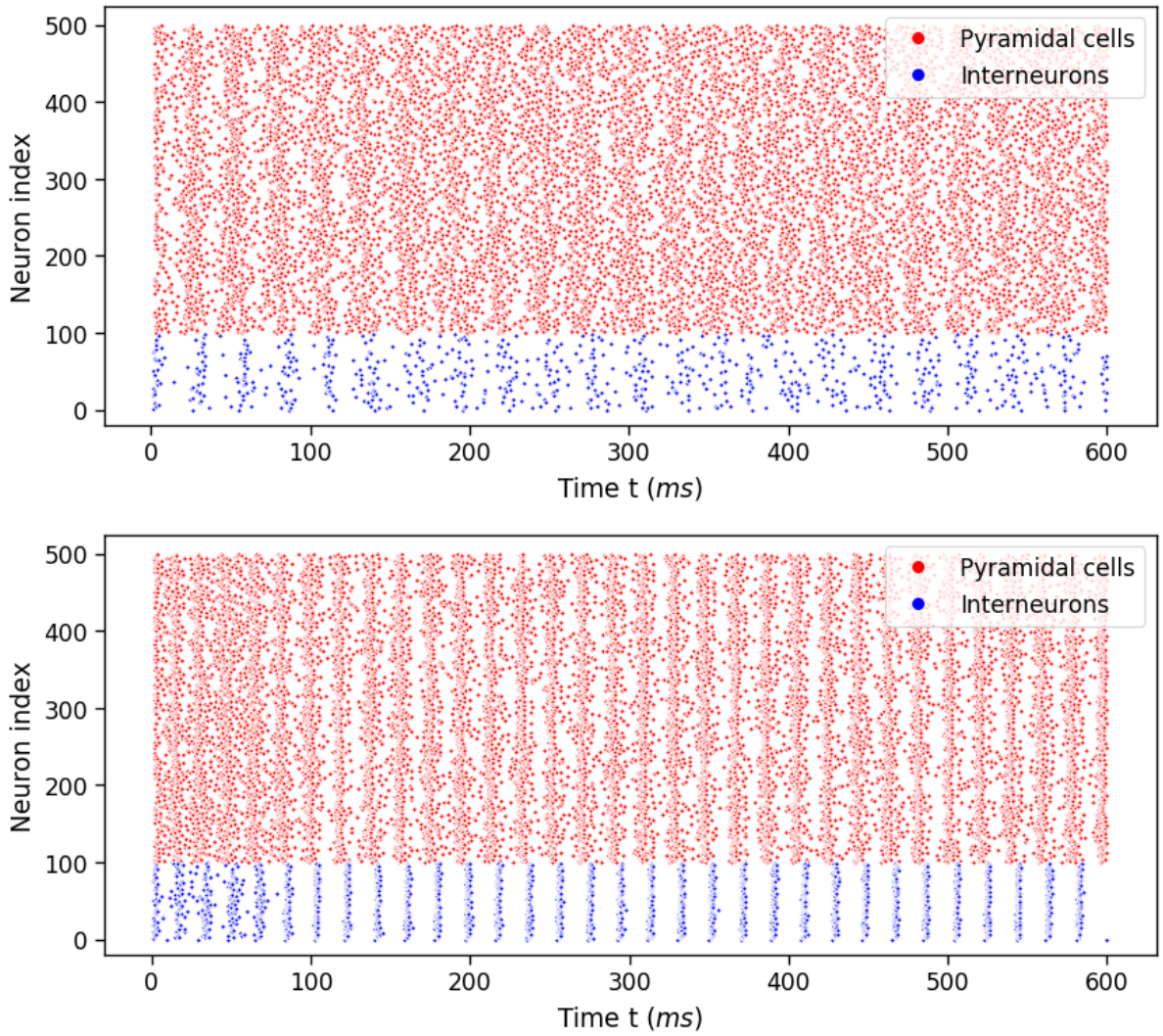

Figure A.1: First panel: Spiketrain scatterplot for condition with low injected current and low PPC value ($\sim$0.025). No clear oscillations are observable. **Second panel**: Spiketrain scatterplot for condition with high injected current and intermediate PPC value ($\sim$0.37). Pyramidal cell volleys precede interneuron volleys by a few ms.

A.3 Manipulation of oscillation frequency through synaptic feedforward connections

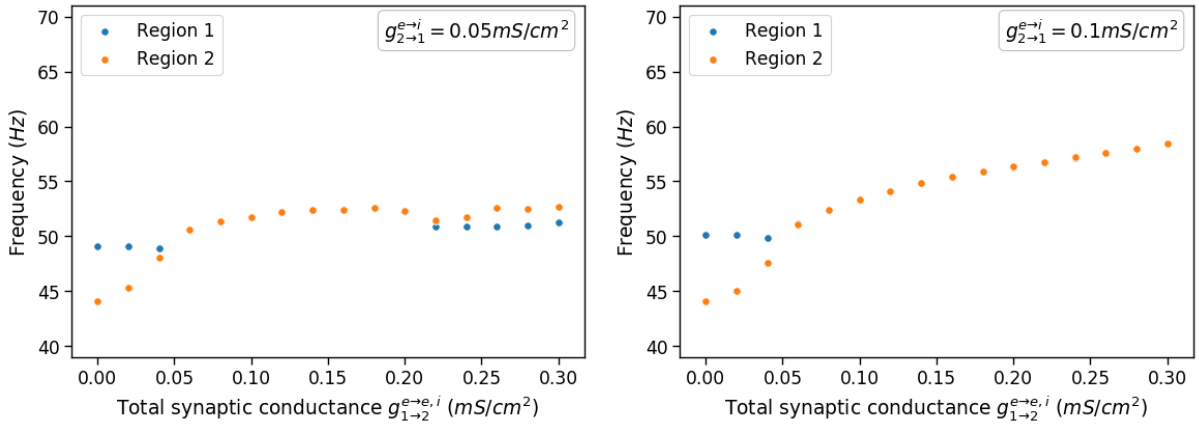

Figure A.2: Frequency of region 1 and 2 as a function of total synaptic conductance. $f_{reg_1} = 47.8$Hz and $f_{reg_2} = 44.2$Hz for both figures. **Left panel**: Feedback $g^{e\to i}_{2\to 1} = 0.05\text{mS/cm}^2$. Region 1 and 2 synchronize for $0.06\text{mS/cm}^2 \leq g^{e\to e,i}_{1\to 2} \leq 0.2\text{mS/cm}^2$. For stronger feedforward connections, they have similar frequencies, both below 55Hz. **Right panel**: Feedback $g^{e\to i}_{2\to 1} = 0.1\text{mS/cm}^2$. Strong feedback induces synchronization between the two regions for $g^{e\to e,i}_{1\to 2} \geq 0.06\text{mS/cm}^2$. The frequency of both increases to up to 60Hz.

A.4 Temporal cross-correlation as a measure of information transfer

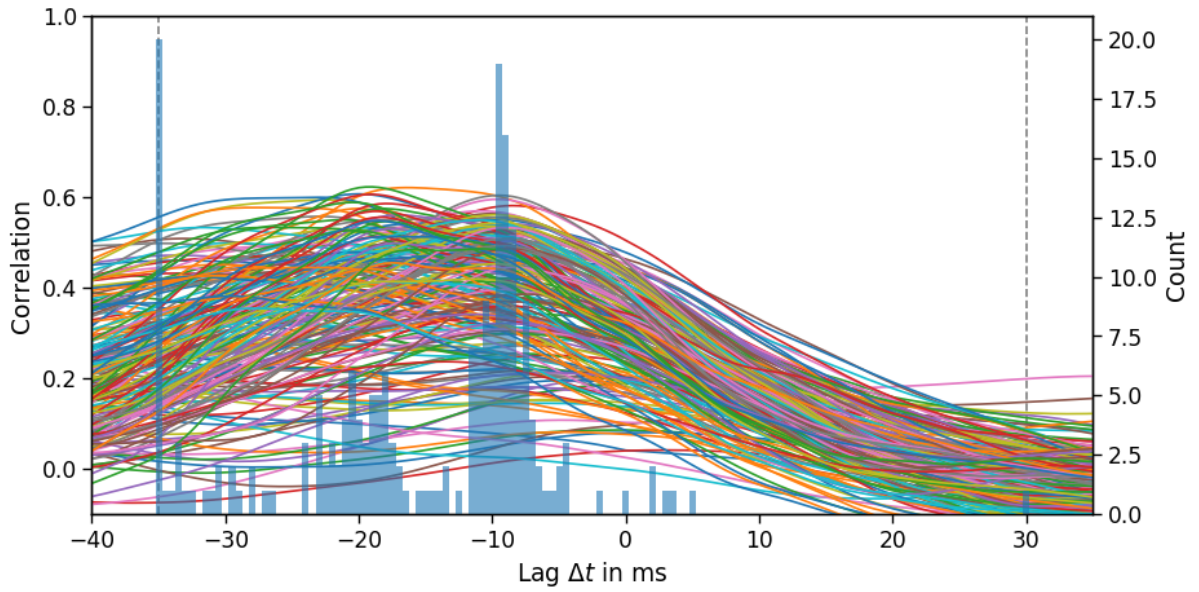

Figure A.3: Cross-correlation between firing rates of region 1 and region 2. The histogram counts how the maxima of the lines are distributed. There is a visible peak of high information transfer at $\Delta t \approx -10$ms. The large bar at -35ms corresponds to very low peaks that indicate little to no information transfer.

A.5 Modulation of coherence through feedback to inhibitory neurons

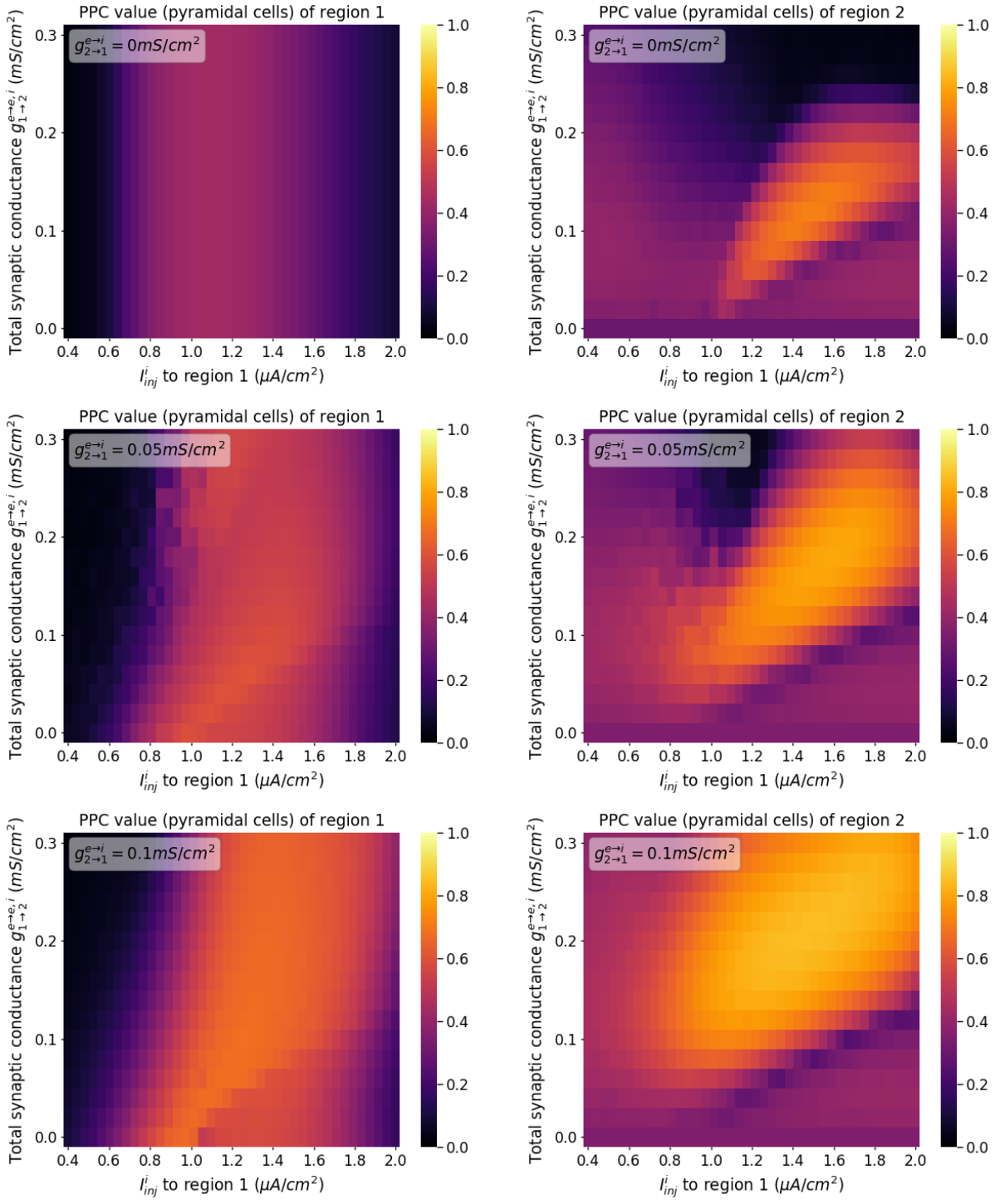

Figure A.4: PPC values for region 1 (left column) and region 2 (right column) as function of feedforward connection strength (y-axis) and injected current to region 1 (x-axis). Intermediary graphs displayed smooth transitions. **First row**: No feedback connections. Phase locking in region 1 is low, region 2 exhibits high values only for conditions of high coherence (cf. Figure 4.3). **Second row**: $g^{e\to i}_{2\to 1} = 0.05\text{mS/cm}^2$. Region 1 phase locking is slightly increased and a faint tilted Arnold tongue appears. Region 2 PPC values increase and in large parts overlap with conditions of high coherence. **Third row**: $g^{e\to i}_{2\to 1} = 0.1\text{mS/cm}^2$. Region 2 displays stable within-circuit synchronization for all conditions.

A.6 Information transfer with feedback to inhibitory neurons

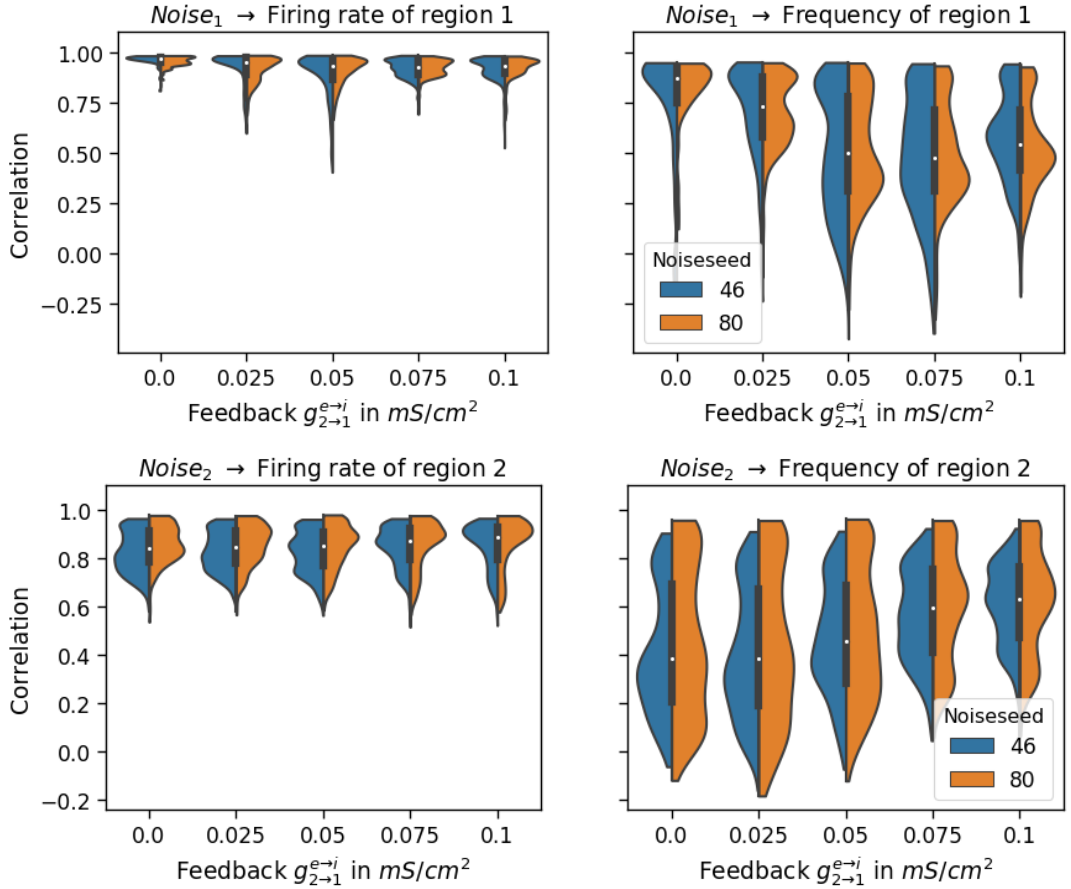

Figure A.5: Comparison of information transfer from noise to region signals. **Upper panel**: Correlation between noise_1 and firing rate (left) or frequency (right) of region 1. High correlation can be observed for the firing rate. For frequency, the information transfer is lower, especially for feedback $\geq 0.05\text{mS/cm}^2$. **Lower panel**: Correlation between noise_1 and firing rate (left) or frequency (right) of region 1. As above, high correlation between noise and firing rate appears. The correlation between noise and frequency is lower, because region 2 is entrained by region 1 in many conditions and can therefore not follow the noise with its frequency. For stronger feedback, the correlation increases.

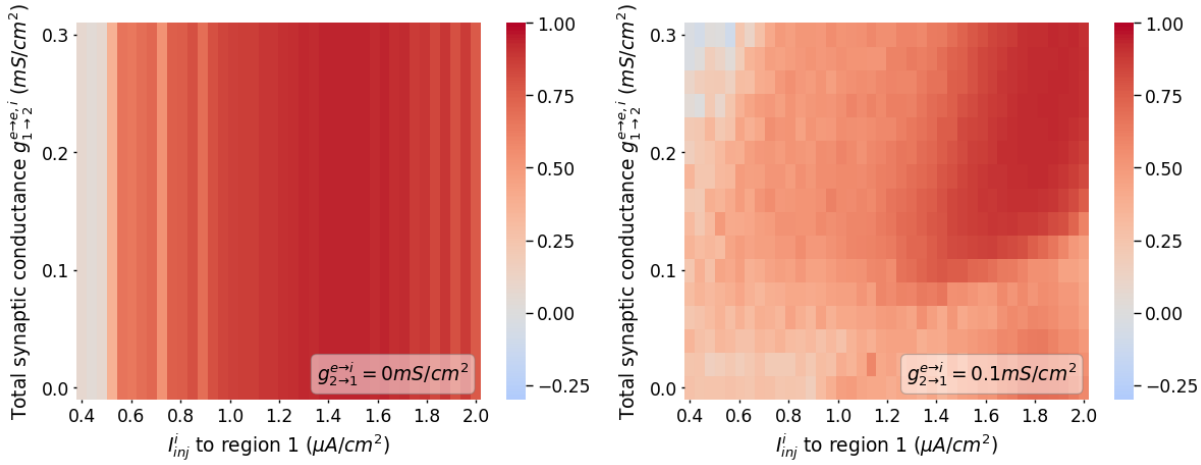

Figure A.6: Correlation between noise_1 and region 1 frequency. **Left panel**: No feedback connections were added. Since the feedforward synaptic conductance (y-axis) does not influence region 1 and no feedback is present, straight lines appear. **Right panel**: Strong feedback ($g^{e\to i}_{2\to 1} = 0.1\text{mS/cm}^2$. The information transfer follows the shape of a tilted Arnold tongue.)

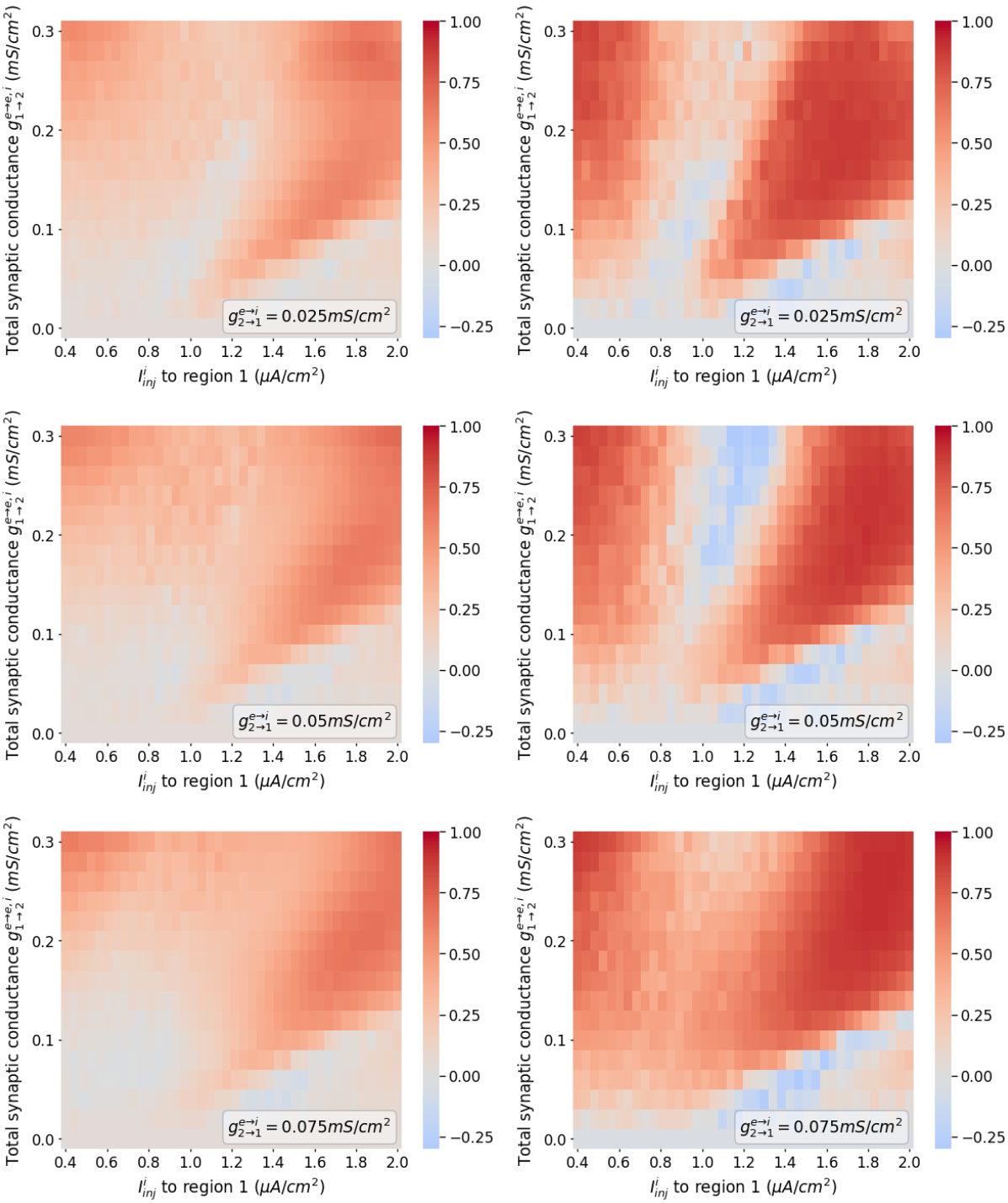

Figure A.7: Intermediary graphs of the correlation between noise$_1$ and region 2 in the firing rate (**left column** and the frequency (**right column**) domain, referenced in section 4.4. **First row**: Low feedback (0.025mS/cm^2) from region 2 excitatory to region 1 inhibitory neurons. The tilted Arnold tongue and the area of slightly higher correlation in the upper left corner are visible. **Second row**: $g_{2\to1}^{e\to i} = 0.05\text{mS/cm}^2$. **Third row**: $g_{2\to1}^{e\to i} = 0.05\text{mS/cm}^2$.

A.7 Digital appendix

This thesis is supplemented by a digital appendix, containing the code used for the simulation and analysis in MATLAB, the functions in python to do further analyses and generate the plots, the settings used for all simulations referenced in this thesis and a documentation which simulation results were used for the figures that appear in this work. It can be found at https://github.com/jzerfowski/bsc_thesis.

matlab/ The entire framework to simulate the behavior of the system. It was adapted from ter Wal and Tiesinga (2017). See `README_old.md` for the original documentation.

matlab/RunScript.m The main script that is run to simulate the network. It uses the settings-files in `matlab/settings_functions/`.

matlab/GridOutput/ The output directory for `RunScript.m`. The simulation results contain over 30GB of data, thus we report the settings including the randomization seeds in `matlab/GridOutput/run_summaries.txt` for reproduction.

matlab/GridOutput/run_summaries.txt Contains an overview over all simulations we ran. First, all categories from `matlab/GridOutput/run_categories.py` are listed. Then, all simulations are listed in numerical order. File generated by `py/generate_summaries.py`

matlab/GridOutput/run_categories.py python dictionary to organize the simulation results into categories. This file is used also by `py/settings.py` to reference the categories.

py/generate_summaries.py Generates the overview on all conducted simulations in `matlab/GridOutput/run_summaries`. We wrote it to easily compare the settings of different runs. To avoid clutter, the script only writes differences to the reference settings in `matlab/GridOutput/reference_settings.mat`.

py/generate_figures.py Calls the function `save_default()` in the `py/figure_*.py`-scripts to automatically generate all figures that appear in this thesis.

figures/ Contains the figures that appear in this thesis.

figures/figures_summary.txt Lists the important details for each figure. E.g., the filename, which simulation runnumbers were used and from which region, condition or timespan the data comes (if applicable).

svg/ The .svg-file and the corresponding .png, depicting the structure of the system.

thesis.pdf This thesis

Declaration of Authorship

I hereby certify that the work presented here is, to the best of my knowledge and belief, original and the result of my own investigations, except as acknowledged, and has not been submitted, either in part or whole, for a degree at this or any other university.

Signature	City, Date